Process Biochemistry

Z. Officinale -Doped Silver/Calcium Oxide Nanocomposites: Catalytic Activity and Antimicrobial Potential with Molecular Docking Analysis

--Manuscript Draft--

Manuscript Number:	PRBI-D-22-00597R1
Article Type:	Full Length Article
Section/Category:	Environmental Biotechnology - Bioremediation, wastewater treatment
Keywords:	Ag/CaO NCs, Green synthesis; Nanoparticles; Antimicrobial activity; Metal oxide nanoparticles
Corresponding Author:	Muhammad Ikram Huazhong Agricultural University, Statistical Genomics Lab PAKISTAN
First Author:	Zakariya Mehmood
Order of Authors:	Zakariya Mehmood
	Muhammad Ikram
	Muhammad Imran
	Anum Shahzadi
	Ali Haider
	Anwar Ul-Hamid
	Walid Nabgan
	Junaid Haider
	Shaukat Hayat
Abstract:	In this study, green synthesized Ag/CaO combined with a reducing agent based on a plant extract was synthesized. Then, the catalytic and antimicrobial potential of extract doped-Ag/CaO was investigated. Bio-reducing synthesis protocol was followed to fabricate Ag/CaO nanocomposites (NCs) by reducing and capping with Zingiber officinale. A series of characterization techniques was employed to examine structural, morphological and optical properties of Ag/CaO. The experimental findings favored doped nanocomposites for use as effective catalysts that degraded toxic dyes such as methylene blue and ciprofloxacin and exhibited strong antimicrobial activity against Escherichia coli (E. coli), and Staphylococcus aureus (S. aueus). Furthermore, a molecular docking investigation determined binding interaction patterns between NCs and targeted cell protein active sites. The obtained results suggested green synthesized Ag/CaO as the most effective inhibitor of dihydrofolate reductase, DNA gyrase, and FabB enzymes. Findings revealed highly economical, non-toxic, and readily available Z. officinale rhizome extract as a potential capping agent to fabricate Ag/CaO for potential applications to reduce major economic losses in the dairy industry for the first time in Pakistan.
Suggested Reviewers:	Dayong Wu dayongwu@mail.ipc.ac.cn
	Muhammad Maqbool mmaqbool@uab.edu
	Khalid Nadeem Riaz khalidbzu@gmail.com
Response to Reviewers:	Reviewer #1: The manuscript investigated the nanocomposite and their antimicrobial as well as catalytic reduction mechanism. 1. There are several typographical mistakes as well in whole manuscript. Therefore, the author's thoroughly careful check the language and typo mistake to minimize the error. Ans: Corrected typos and other errors throughout the manuscript.

2. The abstract should be beginning with a sentence about the background of concept and the aims as well as novelty of study should be mentions. What exactly is the novelty of this study? The abstract is poorly written and should be improved. Abbreviations must be avoided in abstract. Parenthesis should be avoided in abstract - this is poor writing. Please improve.
Ans: The novelty of this research article has been added in the abstract as well as in the introduction section on page 4.

3. Introduction; Check and format the citations in the whole manuscript. Also, appropriate references must be provided to explained the background, what is already done and why this study carried out. Other vise the novelty of this research is still poorly presented. This is important especially for the high IF journals. The scientific style should be used. What exactly is the aim of this work? Hypothesis statement is missing in the introduction section.
Ans: Thanks for the constructive comment. Novelty, as well as a hypothesis, has been incorporated in the manuscript text on page no 4.

4. Results and discussion; General remark to the discussion - In my opinion, the discussion provided by Authors is difficult to follow and verify due missing critical details in the methodology section. Due to poorly described material and poorly presented methods, I am not able to follow and properly review the discussion. I would suggested to add following recent literature in the manuscript.
https://doi.org/10.1016/j.chemosphere.2021.133056;
https://doi.org/10.1016/j.colsurfb.2019.110734;
https://doi.org/10.1016/j.ijbiomac.2021.05.202; and https://doi.org/10.1007/s10529-020-02795-3;
Ans: As per recommendation, we have added these references in the manuscript.

5. All figures are of poor technical quality and not suitable for publication, especially in a high reputed journal. Font size and kind is too small and must be unified in all figures. Small writings are unreadable. All figures must be self-explanatory. Axis titles are poorly presented or absent. Units are missing. Are the data presented in figures significantly different? At least error bars should be shown.
Ans: The quality of all figures has been improved by increasing the font size for easy and better understanding. We have also added bars in figure 5

6. I suggest first time write full name rather than abbreviation; revise throughout in manuscript
Ans: The full description of each abbreviation for the first time throughout the manuscript has been added.

Reviewer #2:
-The article's grammar and punctuation are not adequate and it needs to be deeply proofread.
Ans: Corrected accordingly per suggestions

-Going into details on the specific issues, here some comments are reported:
-All figure captions should be written in clear captions and mention results and discussion also. Some figures (supplementary documents) with results and discussions were not matched.
Ans: As per suggestions, all figure captions in the manuscript have been changed

-In Figure 2. The author should mention clear sample names.
-Figure 2 (a) XRD patterns……. (b) FTIR spectra……. and (c-d) SAED patterns of pristine CaO and extract doped Ag/CaO NCs and (e) representation of the unit cell of Ag/CaO.
Ans: For better and easy understanding, we have mentioned the name of each sample as per above recommendation.

In FTIR Figure2 should indicate significant peak values.
Ans: The significant peak values have been indicated in figure 2.

-The author noted 2.6 characterizations, The visual characteristics of materials were

	studied using a UV-vis spectrophotometer (Genesys 10S) in the wavelength spectrum of 180-400 nm. But the resulting graph In Fig. 3a. Ag exhibited a high peak window at 340-540 nm with maxima at 440 nm? Ans: Thanks for the correction. In 2.6, the wavelength of UV-Vis spectrophotometer (Genesys 10S) has been corrected according to the resulting graph. Figure 4 HR-TEM and interlayer d-spacing images of undoped CaO, Ag and extract doped Ag/CaO NCs. Ans: Thanks for the correction. The caption of figure 4 has been changed for clear understanding. (Fig. S1 (a- d)). But the figure shows the e and f also what about that figures? Ans: Thanks for the correction. The caption of figure S1 has been changed for clear understanding. Figure S1 EDS analysis of pure CaO, Ag and extract-doped Ag/CaO NCs. which is the pure Ans: In figure, S1 (a) represents the pure CaO meanwhile, S1 (b) for pure Ag, S1 (c) for Ag-doped CaO, and (d-f) for 2 mL, 4 mL, and 6 mL extract doped Ag/CaO -Antimicrobial effectiveness of Ag/CaO containing various concentrations of extract was obtained from zone of inhibition (ZOI) measurements through agar well diffusion assay against S. aureus (G +ve) and E. coli (G -ve) pathogens as shown in Fig. S4 but figure shows Figure S4 Schematic diagram of antimicrobial mechanism. What about the ZOI? Ans: Corrected in the manuscript text.

Dear Editor and Referees:

We are resubmitting our manuscript PRBI-D-22-00597 and very thankful to the reviewers for the critical assessment of our manuscript. Keeping in view their critique, we have made careful modifications to the original manuscript. All corrections are marked in the revised manuscript and the explanation to the reviewers' comments are listed in a separate "Answers to the reviewers' comments" document. We believe that the manuscript has been greatly improved and hope it has reached your Journal's standard.

Sincerely,

Dr. Muhammad Ikram

Solar Cell Applications Research Lab, Department of Physics,

G. C. University Lahore, Punjab Pakistan

Z. Officinale-Doped Silver/Calcium Oxide Nanocomposites: Catalytic Activity and Antimicrobial Potential with Molecular Docking Analysis

Zakariya Mehmood[a], Muhammad Ikram[a*], Muhammad Imran[b], Anum Shahzadi[c], Ali Haider[d], Anwar Ul-Hamid[e*], Walid Nabgan[f*], Junaid Haider[g], Shaukat Hayat[h]

[a]Solar Cell Application Research Lab, Department of Physics, Government College University Lahore, Lahore, 54000, Punjab, Pakistan

[b]State key Laboratory of Chemical Resource Engineering, Beijing Advanced Innovation Centre for Soft Matter Science and Engineering, Beijing Engineering Centre for Hierarchical Catalysts, Beijing University of Chemical Technology, Beijing 100029, China

[c]Faculty of Pharmacy, The University of Lahore, 54000, Lahore, Pakistan

[d]Department of Clinical Sciences, Faculty of Veterinary and Animal Sciences, Muhammad Nawaz Shareef, University of Agriculture, Multan, 66000, Punjab, Pakistan

[e]Core Research Facilities, King Fahd University of Petroleum & Minerals, Dhahran, 31261, Saudi Arabia

[f]School of Chemical and Energy Engineering, Faculty of Engineering, Universiti Teknologi Malaysia, 81310, Skudai, Johor, Malaysia

[g]Tianjin Institute of Industrial Biotechnology, Chinese Academy of Sciences, Tianjin 300308, China.

[h]Department of Physics, Riphah Institute of Computing and Applied Sciences (RICAS), Riphah International University, 14 Ali Road, Lahore, Pakistan

*Corresponding authors emails: [a]dr.muhammadikram@gcu.edu.pk, [e]anwar@kfupm.edu.sa, [f]wnabgan@gmail.com

ABSTRACT

In this study, green synthesized Ag/CaO combined with a reducing agent based on a plant extract was synthesized. Then, the catalytic and antimicrobial potential of extract doped-Ag/CaO was investigated. Bio-reducing synthesis protocol was followed to fabricate Ag/CaO nanocomposites (NCs) by reducing and capping with *Zingiber officinale*. A series of characterization techniques was employed to examine structural, morphological and optical properties of Ag/CaO. The experimental findings favored doped nanocomposites for use as

effective catalysts that degraded toxic dyes such as methylene blue and ciprofloxacin and exhibited strong antimicrobial activity against *Escherichia coli (E. coli),* and *Staphylococcus aureus (S. aueus).* Furthermore, a molecular docking investigation determined binding interaction patterns between NCs and targeted cell protein active sites. The obtained results suggested green synthesized Ag/CaO as the most effective inhibitor of dihydrofolate reductase, DNA gyrase, and FabB enzymes. Findings revealed highly economical, non-toxic, and readily available *Z. officinale* rhizome extract as a potential capping agent to fabricate Ag/CaO for potential applications to reduce major economic losses in the dairy industry for the first time in Pakistan.

Keywords: Ag/CaO NCs, Green synthesis; Nanoparticles; Antimicrobial activity; Metal oxide nanoparticles

1. INTRODUCTION

Unrestricted use of dyes in industrial sectors such as paper, polymer, wood, food and textiles may result in immense environmental pollution [1, 2]. Among these dyes, most are potentially toxic to humans, animals, and plants. They may inflict serious ailments, including liver malfunction, skin cancer, allergy, etc. [3]. Methylene blue (MB) is highly toxic and hazardous, which can cause mutation in the biosphere. Therefore, it is vital to degrade and eliminate pollutants from the environment, especially water. The published literature suggests various methods to safely remove such dyes including photo-degradation, reverse osmosis, coagulation, and chemical reduction [4, 5]. The chemical reduction method used for organic dye degradation relies upon a potent reducing agent accompanied by noble metals platinum (Pt), gold (Au), silver (Ag), and copper (Cu) [1, 6, 7]. However, catalysts produced using noble metals are generally too expensive for practical applications. Therefore, synthesizing nanocatalyst with non-noble metal such as calcium (Ca) is attractive since it exhibits performance comparable to noble metals, however, at a relatively far diminished cost [8, 9].

The development of resistance in bacteria against conventional antibacterial drugs due to its non-essential and excessive use is a major global concern. The situation calls for the adoption of new approaches that can appease the emerging predicament. In this respect use of natural products has great potential due to their unmatched chemical diversity. Both pure compounds and standardized plant extracts can be employed for developing novel drugs. Many researchers have diverted their attention toward traditional medicine to develop active drugs

to combat microbial infections [10]. It is generally assumed that plants employed in traditional medicine have low toxicity. However, the harmful ramifications of commonly used herbs must be thoroughly established for long-term usage. Recent in vitro studies found that a number of plants used as food or in traditional medicine are mutagenic. Mutagenesis potential of plants has raised concerns for their long-term usage [11]

Until now, metal oxide nanoparticles (MONPs) were successfully fabricated via physiochemical methods; however, such approaches are costly and associated with the use of hazardous reagents. Contemporary risks to the environment caused by toxic organic solvents combined with high pressure employed during their synthesis limit their medical applications [1, 12]. Therefore, green synthesis has overwhelmingly become a research focus for bio-reduction of MONPs in the past decade since the plant-based MONPs promise a brilliant outlook in the fields of cosmetics, pharmaceuticals, and food [13]. MONPs are also synthesized using plant tissue and other parts since the plant extract-based method is more rapid, efficient, and suitable for large-scale production [14]. Plant extract-based method can also be carried out at room temperature (non-thermal method). Jaewook et al. synthesized Au nanoparticles (NPs) non-thermally with stability akin to thermal synthesis protocol [15]. Similarly, Mallikarjuna et al. fabricated silver and palladium crystals at room temperature (non-thermal method) using tea and coffee extract. The product showed promising stability and typical green synthesis attributes [16, 17].

Currently, iron (Fe), Zinc (Zn), Ag, Cu, calcium (Ca), etc., NPs are synthesized using biosynthesis for different applications. Calcium oxide (CaO) NPs have a unique crystalline structure, optical properties, and exhibit exceptional antimicrobial activity. They are non-toxic, making them safe for use in biomedical, electronics, environmental remediation, sensors, and catalysis applications [18-20]. For centuries, Ag has remained a well-known antibacterial agent as it works in a unique way such that Ag^{+} destroys cell membrane and replication ability of microbial DNA [19, 20]. Besides, these are also employed as antiseptics, disinfectants, and as pharmaceutical agents [22, 23]. Ginger (*tuberous rhizome*) is cultivated worldwide to be used as a spice and medicinal ingredient [24]. It holds 400-plus compounds, including gingerol and shogaol, that exhibit various physiological and pharmacological attributes such as anti-inflammatory, anti-apoptotic, anti-tumorigenic, anti-hyperglycaemic, and anti-emetic properties [25]. The combination of Ag/CaO makes it very efficient and promising for use in catalysis and antimicrobial activity. The nanocomposites (NCs) are

much more biocompatible than Ag NPs alone. Moreover, they are significantly less toxic while disclosing high antibacterial activity. They are comparatively very efficient and, at the same time, inexpensive antimicrobial materials [26]. A study also showed that Ag/CaO is effective in seizing the proliferation of microorganisms, which makes them useful in applications that involve contact with human skin [27]. Furthermore, the NCs are an excellent catalyst against many industrial dyes. A study was conducted in this respect, which revealed that NCs are not only efficient but also very resilient and stable; they did not alter even after five consecutive cycles of use. Moreover, it is logical to synthesize such a structure that has a biocompatible component (i.e., CaO) and as well as the best antimicrobial agent that possesses the attributes of each as whole. The study was carried out against 4-Nitrophenol to be reduced in water from natural resources. The results revealed NCs to be very promising and effective as a potential catalyst for the treatment of industrial wastes [28].

In view of the aforementioned attributes, each aspect of this study of the metal/metal oxide NCs was designed to preserve the antimicrobial action and dye degradation capability of the individual material and enhance the biocompatibility NCs as a whole. In this study, highly economical, non-toxic and readily available fresh ginger *Zingiber officinale* (*Z. officinale)* rhizome extract was used as a capping and reducing agent to fabricate Ag/CaO NCs with potential antimicrobial application against pathogenic isolates of *S. aureus* and *E. coli* isolated directly from mastitic milk to reduce dairy industry economic losses. The catalysis of non-noble metallic catalyst was checked in the presence of $NaBH^{-4}$ against methylene blue and *ciprofloxacin* (MB:CF), common industrial dyes, with the hypothesis that as-fabricated NCs would efficiently reduce bacterial growth and clean industrial dyes from wastewater. The result showed that the dyes were degraded up to 100%. Additionally, in silico docking investigations were conducted against specific enzyme targets from *Escherichia coli (E. coli),* and *Staphylococcus aureus (S. aueus),* correspondingly.

2. Materials and Methods

Calcium chloride dihydrate ($CaCl_2.2H_2O$, 99%), silver nitrate ($AgNO_3$, 99.8-100.5%), and sodium hydro oxide (NaOH, 98%) were bought from Sigma-Aldrich (Germany). Fresh roots of *Z. officinale* were purchased from a market located in Lahore (Pakistan) and shade-dried to attain invariant weight prior to further processing. The media used for bacterial growth in this investigation were of analytical grade.

2.2. Extract Preparation

Fine powder of *Z. officinale* root was achieved through grinding in an electric grinder, and subsequently preserved in the plastic container. Post grinding, a certain quantity of deionized water (DIW) (1:10) was poured into the powder and stirred vigorously for 30 minutes (min) at 70 °C. When extract became chilled, filtration was carried out using Whatman No. 1 filter paper. The obtained extract was preserved at 4 °C to avoid fungal production (Fig. 1a) [29].

2.3. Synthesis of bare and extract doped Ag/CaO NCs

An aqueous solution containing 35 mL DI water as soluble, $CaCl_2.2H_2O$, and $AgNO_3$ (4.9 g and 0.25 g) were stirred for 5 min at 90 °C on a hot plate. Subsequently, ginger extracts of different quantities (2 mL, 4 mL, and 6 mL) were poured into three separate pure solutions in the form of drops while keeping the fourth as reference. Meanwhile, NaOH solution (0.5 M) was incorporated to retain pH ~ 12. The colloidal solution was vigorously stirred at 90 °C for 2 hours [19, 24]. Consequently, the precipitate formed was washed and centrifuged at 7100 rpm for 9 min. Finally, the precipitate was calcinated at a constant temperature of 90 °C inside the oven until the water thoroughly evaporated (Fig.1b).

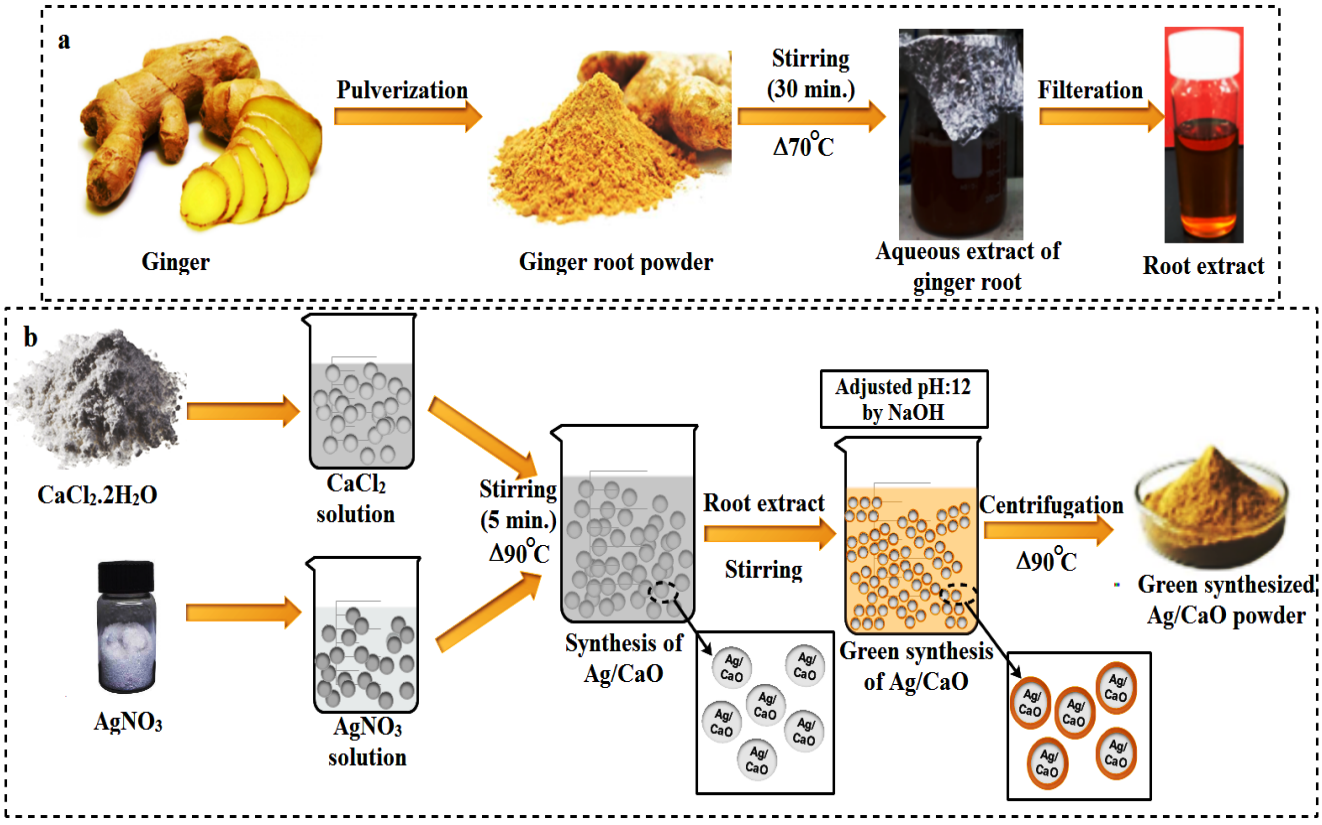

Figure 1 Schematic diagram of (a) extraction of ginger root and (b) synthesis of green synthesized Ag/CaO NCs.

2.4 Isolation and Identification of *S. aureus* and *E. coli*

Specimens of ovine milk from veterinary facilities in Punjab, Pakistan, were raised on 5 percent sheep blood agar and reared at 37 °C for 24-48 hours [30]. The standard colonies acquired were extended into three isolated *S. aureus* and *E. coli* on manitol salt (MS) and MacConkey agars (MA), respectively [31]. Burgey's determinative bacteriology manual established gram's staining, while coagulase and catalases tests were adopted for morphological and biochemical confirmation of refined cell colonies.

2.4.1 Antibacterial evaluation

Antibacterial performance of all doped materials was assessed utilizing the well diffusion technique through swabbing 1.5 $\times 10^8$ CFU/mL *S. aureus* as Gram-positive (G +ve) and *E. coli* as Gram-negative (G –ve) on MS and MA plates, separately. Bacterial isolates were swabbed on agar plates and 6 mm diameter wells were derived using a sanitized borer. Each well was infused with a different quantity of Ag/CaO containing varying concentrations of extract (2, 4, and 6 mL) 0.5 and 1.0 µg/50 µl and segmented using ciprofloxacin (0.005 µg/50 µL) and DIW (50 µL) as control positive (+ve) and negative (-ve), correspondingly. Antibacterial effectiveness was assessed by quantifying inhibitory regions in millimeters (mm) after overnight incubation of loaded agar plates at 37 °C using a Vernier calliper.

2.4.2 Statistical Analysis

One-way analysis of variance (ANOVA-1) was used to statistically determine antibacterial effectiveness represented by diameter of inhibition zone (mm) through a statistical package for social sciences (SPSS 20).

2.5. Molecular Docking Analysis

To better understand the mechanism underlying bactericidal action, molecular docking analysis of green synthesized Ag/CaO nanoparticles was conducted. Aside from Ag/CaO nanoparticles, Zingerone (ZGN) and Shagoal (SGL), the major compounds of *Z. officinale*, that make complexes with nanoparticles were selected for molecular docking studies [32,33] (Fig. S6). This was accomplished by focusing on proteins that are essential for bacterial durability and development. Many targets of protein associated with discrete biosynthetic pathways were selected for docking analysis specifically, DNA gyrase$_{S.\ aureus}$, dihydrofolate reductase (DHFR), and DNA gyrase$_{E.\ coli}$ and β-ketoacyl- [acyl carrier protein] synthase I (FabB). DNA gyrase and DHFR are essential for the biosynthesis of DNA and folic acid, which are both required for bacterial viability. FabB also catalyzes crucial steps in the

bacterial cell's fatty acid biosynthetic pathway [34–36]. A protein data library was used to obtain crystallographic structures of target proteins from *E. coli* and *S. aureus* (Fig. S5). The 3D-structure of DNA gyrase$_{s.aureus}$ (PDB ID: 5CTU), resolution: 1.45 Å [37], dihydrofolate reductase (PDB ID: 3FY8), resolution: 2.20 Å [38], DNA gyrase B$_{E. coli}$ (PDB ID: 4PRV), resolution: 1.45 Å [39] and β-ketoacyl- [acyl carrier protein] synthase I (FabB (PDB ID: 1FJ4),), resolution: 2.35 Å [40] were searched from protein data bank.

Molecular docking analysis was carried out using SYBYL-X 2.0 program [41]. Sybyl-X2.0/SKETCH module was used to create 3D structures of selected compounds [42], followed by energy minimization using the Tripos force field with Gasteiger Hückel atomic charge [43]. The Surflex-Dock module of the molecular modelling software programme SYBYL-X 2.0 [43] was used to analyze flexible molecular docking simulations to study binding interactions of nanoparticles with active site residues of selected proteins. Missing hydrogens were introduced. According to the AMBER 7 FF99 force field, atomic types were allocated, and atomic charges were applied. Finally, using the Powell algorithm with a convergence gradient of 0.5 kcal//(mol · A) for 1000 cycles, the energy was reduced to avoid steric clashes. For each ligand-receptor complex system, at least 20 of the finest docked poses were saved conclusively. The Hammerhead scoring system was used to rate the best putative ligand poses. Surflex dock module generates and ranks putative poses of ligand fragments using an empirically generated consensus scoring (cScore) [44] function, that combines Hammerhead's empirical scoring function [45], comprised of , D-score (dock score), G-score (gold score), Chem-Score, potential mean force (PMF) score, and/or complete score, with a molecular similarity method (morphological similarity).

2.6 Characterization

The structural and crystalline characteristics of the generated NCs were investigated using XRD diffractometer (PAN Analytical X'pert PRO type x-ray diffractometer) and monochromatic Cu-K radiation (λ = 1.5418 Å) at a scanning speed of 5°/min across a two-degree range of 5° to 80°. Infrared spectroscopy was performed with Excalibur 3100 spectrometer in spectral region 4000-400 cm^{-1}. The morphological features, size of the nanoparticles and specimens layer spacing were assessed using a scanning electron microscope (SEM), JEOL JSM-6460LV and JEOL JEM-2100F high-resolution transmission electron microscopes (HR-TEM). The visual characteristics of materials were studied using a UV-vis spectrophotometer (Genesys 10S) in the wavelength spectrum of 270-650 nm. The

photoluminescence (PL) spectra of doped materials were acquired using a spectrofluorometer (JASCO, FP–8300). X-ray photoelectron spectroscopy was used to evaluate the specimen composition and related band gaps (XPS).

2. RESULTS AND DISCUSSION

To acquire information regarding phase, structure, and crystal size of extract-doped and un-doped Ag/CaO NCs, the CaO and Ag NPs were examined using XRD technique. Obtained patterns are shown in figure 2a, which contains all the necessary peaks of CaO in the respective samples. The peaks were observed in pure Ag and Ag/CaO samples at 38.8° and 44.8° with (111) and (200) crystal planes, while the peak at 56.2° (142) disappeared in the Ag/CaO sample. A large reduction in peak intensity occurred due to the lower concentration of Ag in Ag/CaO samples. The peaks flexing at ~28.59°, 31.9°, and 47.01°corresponding to (210), (111), and (112) planes, respectively, originated from CaO in Ag/CaO and pure CaO samples. A cubic structure was exhibited without any impurity traces corresponding to JCPDS card No. 00-004-0777. Most of the peaks that had minor intensities standing at 29.54°, 36.01°, 39.44°, 43.17°, 48.52°, and 62.59° were confirmed as (104), (110), (202), (018), (116), and (300) crystal planes. This group of bands belonged to CaO appearing as $CaCO_3$ in JPCDS card (File No. 47-1743) [46, 47]. Recorded data also contained a few highly intense peaks flexing at 18.05°, 34.09°, and 50.90° attributed to (001), (101), and (110) planes, respectively. These peaks corresponded to $Ca(OH)_2$ (PDF Card No. 00-087-0673), the responsibility of observed OH^- existence given to moisture in air and DIW insertion. The patterns revealed NPs to be crystalline by nature. The sizes of crystallites were determined from XRD patterns with the help of Scherrer formula. Computed crystallite sizes were 29.66, 28.64, 28.64, and 26.00 nm for pristine, 2, 4, and 6 mL samples, respectively. As it can be observed, the size of crystallites varied with different concentrations of extract while carrying different phytochemicals used as reducing and capping agents, which determines the average crystallite size of MONPs [48, 49].

The vibrational characterization study of infra-red responsive functional groups of CaO, Ag, and Ag/CaO NCs were undertaken with FTIR spectroscopy. Fig. 2b revealed (O-H) stretching at 3637 cm^{-1} that was probably influenced by DIW and moisture in air. Peak flexing at ~1630 and 3370 cm^{-1} corresponded to N-H bending and stretching, respectively, in Ag spectrum. Two bands, 821 and 1014 cm^{-1} were attributed to metabolites and protein functional groups that cover Ag NPs. A strong band of absorption occurred at 1439 cm^{-1} for

which the carbonyl (C=O) group was responsible. This occurs due to rapid absorption of CO_2 in atmosphere by calcium hydride, which transforms it into $CaCO_3$ [50, 51]. The absorption peak standing at 1062 cm^{-1} corresponded to (C-O) stretching indicating alcohol presence [51]. The medium absorption band at 872 cm^{-1} mirrored the existence of C–H for Ag/CaO NCs [52]. The band near 607 cm^{-1} revealed the presence of capping agents and NPs [50]. No significant shift occurred with extract doping, however, intensities did change. The FTIR spectrum of biosynthesized from ginger is manifested in Fig. 2 b. The broad absorption band ~ 3039 cm^{-1} corresponds to OH meanwhile, peak broadening revealed carbonyl groups with (N-H) amine stretching frequency. Observed FTIR peaks around 2592 cm^{-1}, 1880 cm^{-1}, 1495 cm^{-1}, and 1346 cm^{-1} corresponded to CH_2-CH_3, CH_2-OCH_3, and C-OH functional groups, respectively, which presented α-Zingeberene, 6-gingerol, and 6-snogal of *Z officinale* [51,52] . Selected area electron diffraction (SAED) analysis of pure and extract doped Ag/CaO NCs were obtained on a small portion inside the sphere as shown in Fig. 2c-e. The obtained result displays concentric circles, which indicate poly-crystallinity of NCs. Diffraction rings inside SAED were ascribed to (001), (101), (110), (111), (220), and (311) planes which were indexed as face-centered cubic (FCC) $Ca(OH)_2$ and CaO, and were found to be consistent with XRD analysis.

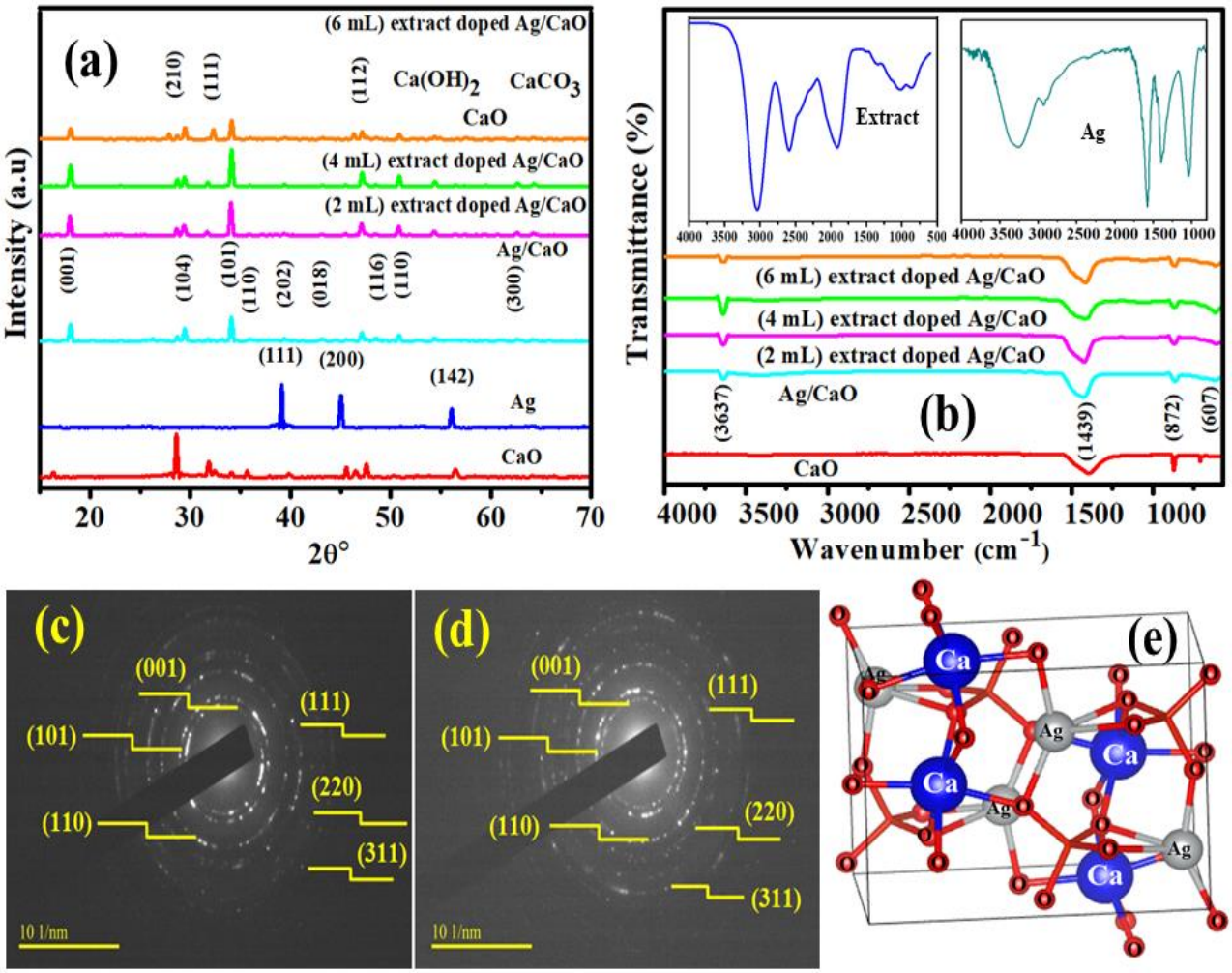

Figure 2 (a) XRD patterns CaO, Ag, Ag/ CaO, and (2, 4, and 6 mL) extract doped Ag/CaO (b) FTIR spectra CaO, Ag/CaO and (2, 4, and 6 mL) extract doped Ag/CaO, respectively (inside Extract and Ag), (c-d) SAED patterns of pristine CaO and 6 mL extract doped Ag/CaO NCs and (e) representation of the unit cell of Ag/CaO.

Initial confirmation of NCs formation was acquired by studying optical properties through UV-vis spectroscopy. The obtained spectra of CaO, Ag, Ag/CaO, and different concentrations of ginger extract (2 mL, 4mL, and 6 mL) carrying Ag/CaO NCs are plotted in Fig. 3a. The absorption band for CaO was recorded at 290-340 nm. Ag exhibited a high peak window at 340-540 nm with maxima at 440 nm. Pure Ag/CaO shows a similar weak absorption like CaO, affected by complete absorption of Ag-NPs into $CaCO_3$ crystallites [46,47]. Absorption was drastically enhanced upon adding extract to pure Ag/CaO and increased with extract concentration. The maximum absorption was recorded for a sample carrying 6 mL extract. Absorption increase is probably affected by an upsurge in absorption species influenced by surface plasmon resonance (SPR) excitations. The maxima of absorptions for NCs carrying 2 mL, 4 mL, and 6 mL extract were found at 428, 412, and 406

nm, respectively. Blueshift could be observed by increasing extract to high concentrations, respectively. The shift is affected by the donation of electrons to the particles. Upon injection of holes to clusters the redshift occurs, plasmon shifts occur when a bare cluster has positive and negative charges [53,54]. It is observed from the results that by increasing the ratio of extract concentration, the concentration of reducing agents in the reaction medium increased, as a result, electron density further increased. The reducing agent contains charged groups that would restrict free electrons near Ca and Ag clusters inside a restricted volume which results into an increase in charge on the surface of clusters. Interaction of these increased charges with the surrounding reducing medium accounts for particle size decrease [55]. The band gap energy values calculated through Tauc's plot were 2.93 eV, 3.02 eV, 3.18 eV, and 3.25 eV for reference, 2 mL, 4 mL, and 6 mL samples, respectively (Fig. 3b).

In addition to UV-Vis, photoluminescence spectroscopy (PL) was employed to evaluate optical properties of concerned NCs, specifically charge recombination and half-life of the exciting material in their conductance band. PL emission spectra of undoped and doped Ag/CaO NCs with ginger extract of various concentrations (2 mL, 4 mL, and 6 mL) are shown in Fig. 3c. Data was recorded under 350 nm excitation, which delivered sharp peaks at 412-402 nm, due to band edge excitonic emission [56, 57]. Extremely excited carriers near or in metal NPs probably relax non-radioactively by emitting plasmon [58]. Observed PL spectra display a blueshift which indicated that surface plasmon resonance (SPR) phenomenon occurred contrary to inter-band emission [59]. Mechanism can be elaborated as: incident light contains excited inter-band transitions, whereas excited electrons rest in SPR modes, emitting photons. Since SPR is size-dependent [59], blueshift corresponds to size, which decreases with an increase in extract concentrations, this also matches with UV-Vis results. However, peak intensity shows that recombination rate is not size dependent, but depends upon the polarizability per unit volume [60]. Observed peaks containing high extract concentrations promise a low recombination rate, as confirmed from the graph, which is due to favourable dopant amount acting as a trap for photo-e^- and h^+ pairs, thus further separating the charge carriers [61, 62]. Interband electronic transitions are excited by the incident light. This excitation relaxes into the SPR modes, and the SPR then radiates or emits this energy as photons (radiatively decays).

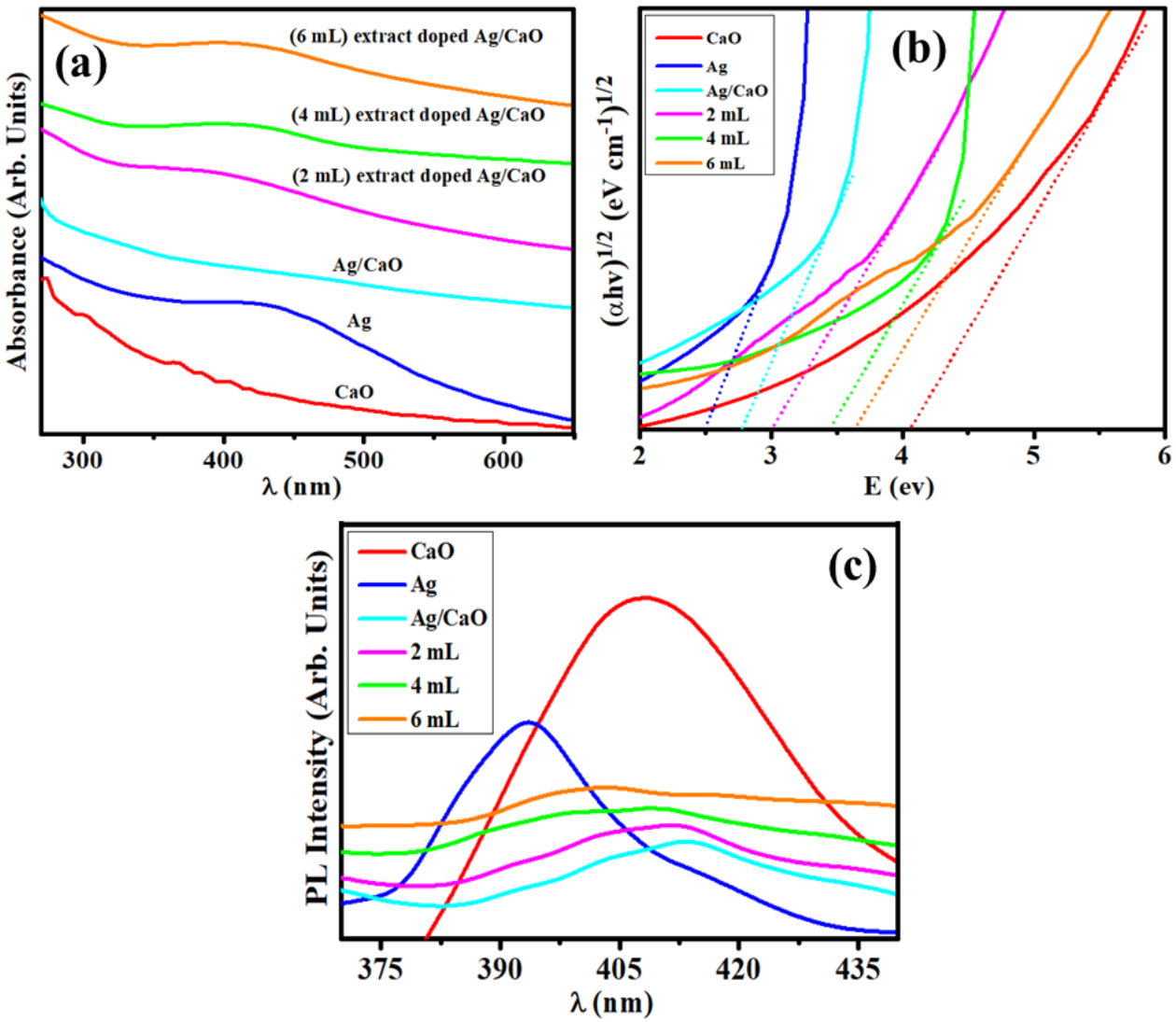

Figure 3 (a) Absorption spectra, (b) using Tauc plot calculated Eg and (c) PL spectra for CaO, Ag, Ag/Ca and (2 mL, 4 mL, and 6 mL) extract doped Ag/CaO NCs, respectively.

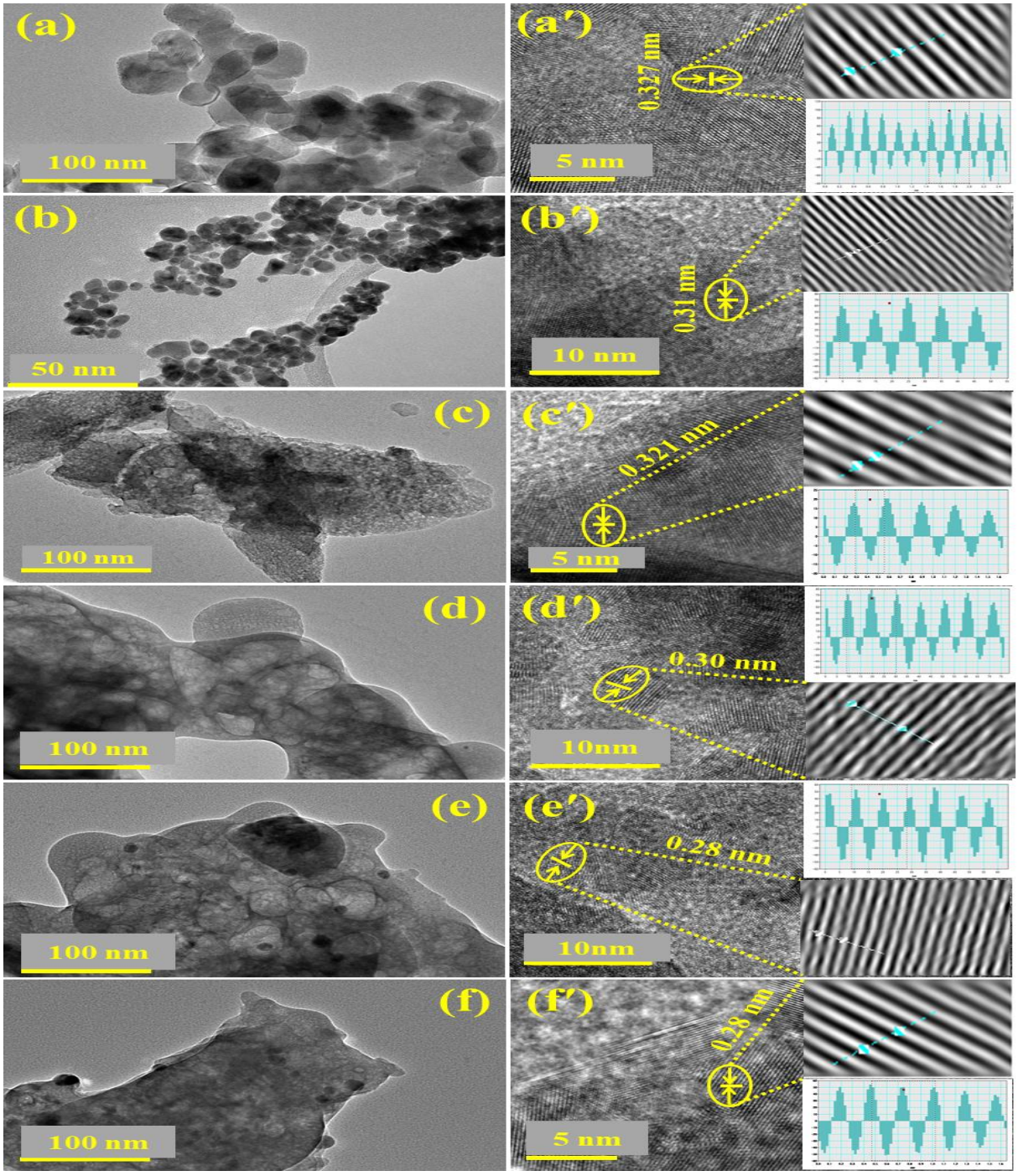

Figure 4 (a-f) HR-TEM and (a′-f′) interlayer d-spacing images of un-doped CaO, Ag, Ag/CaO, and (2 mL, 4 mL, and 6 mL) extract-doped Ag/CaO NCs, respectively.

To study further the structure and differences of microstructure in crystals of CaO, Ag, and un-doped and doped Ag/CaO-NCs, HR-TEM was employed. HR-TEM images disclosed non-uniform nanocrystalline structure of CaO NPs having almost spherical shape with high agglomeration. Ag particles were dispersed and agglomerated simultaneously, which were approximately spherical and faceted in shape. High agglomeration of NCs was observed in

the samples of Ag/CaO with a size roughly < 100 nm since high surface energy is manifested when synthesis is performed in an aqueous solution [63]. Ag NPs of roughly 10–20 nm appeared around the CaO NPs as a result of reduction by extract of salt containing Ag, depicted in Fig. 4 [53]. Phytochemicals in extract-carrying samples were found to exist in the form of a thin layer [64]. HR-TEM rendered the lattice fringes to be 0.327, 0.31, 0.32, 0.30, 0.28, and 0.28 nm for pure CaO, Ag, and 2 mL, 4 mL, and 6 mL, which ascertained the formation of highly crystalline nanostructures. To determine the content of elements and additional features of fabricated NCs, EDS technique was employed. The results disclosed reduction phases of CaO and Ag, confirming the successful completion of desired synthesis (Fig. S1 (a- f)). The spectra possessed two major peaks pertaining to Ca having high purity at 0.4 and 3.8 keV, Ag peak with immense purity was found at 3.1 keV and a single peak that belonged to O at 0.6 keV. Traces of carbon in pristine samples result from the carbon tab onto which the sample was placed during analysis. The spectra also revealed the presence of Na and Cl, Na existence is due to the use of NaOH.

Catalytic efficacy of pristine CaO, Ag, and extract-doped Ag/CaO NCs were checked by using MB:CF, while accompanied by reducing agent sodium borohydride ($NaBH_4$) as shown in Fig. 5. The experiment was carried out by mixing 3 mL of MB:CF with roughly 400 µl $NaBH_4$ prior to adding NCs. It was assured that $NaBH_4$ alone did not affect any degradation. Afterward, 400 µl NCs were added into MB:CF solution and degradation was analyzed using UV-vis spectra. Un-doped CaO, Ag, and doped Ag/CaO NCs with (2 mL, 4 mL, and 6 mL) extract showed different reduction rates in respective time spans. Undoped CaO, Ag, and Ag/CaO exhibited a total (70, 81, and 85%) dye reduction within 20-25 min, respectively, in a neutral medium. Surprisingly, the rest of the samples completely degraded MB:CF. However, time consumption was different which were 2 min, 17 min, and 30s for 2 mL, 4 mL, and 6 mL samples, respectively. The same experiment was repeated for basic and acidic-based solution of MB:CF and $NaHB_4$, which rendered the best results in acidic solution i.e., 75, 88 and 100% degradation within a half min for Cao, Ag, and Ag/CaO doped samples. In the case of basic medium, except for 6 mL sample, which showed 100% instant degradation, CaO, Ag, Ag/CaO, 4 mL, and 2 mL samples breached the dye to 19.2. 10.15, 34.6, 90, and 96% consuming 10 min and no further color change was observed. The control sample delivered the least 30% dye reduction performance in 12 min followed by no further change.

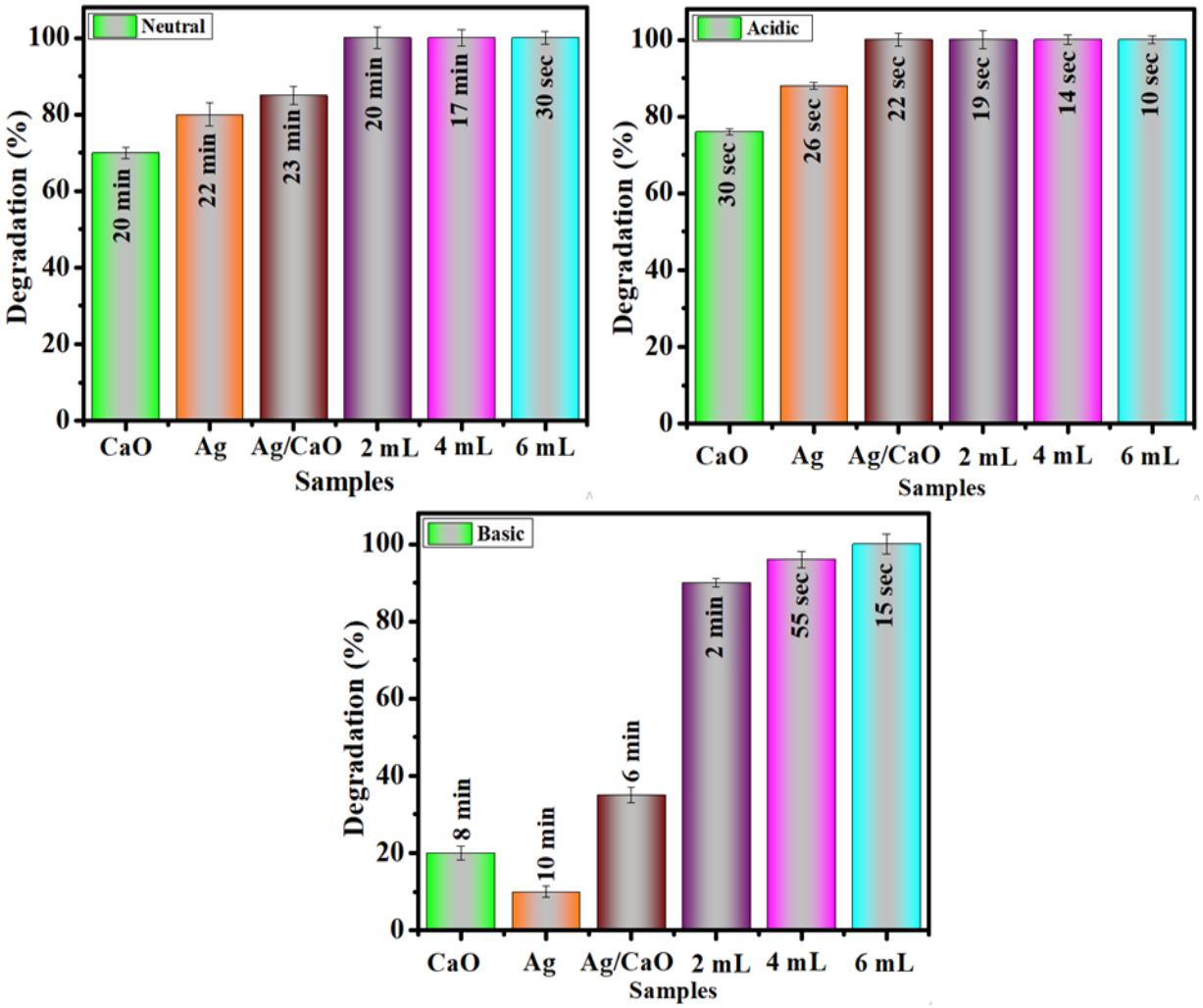

Figure 5 Catalysis of pristine CaO, Ag, Ag/CaO, and (2 mL, 4 mL, and 6 mL) extract doped Ag/CaO NCs in neutral, acidic, and basic medium, respectively.

The phenomenon of dye degradation is well illustrated in Fig. 6, BH_4^- after dissociation of $NaBH_4$ becomes an electron donor which transfers an electron to MB:CF via CaO, Ag, and Ag/CaO NPs (Paul et al. 2020). The most crucial part in dye degradation was played by Ag/CaO NPs, which accept and then transfer the electron [65, 66]. Redox potential reduction occurred with increased Fermi potential, which probably is affected by the size of NPs [7]. Size plays a key role in the potential interfacial barrier, for small particles barrier is small since the surface is larger, and vice versa [7]. In the current study, efficiency and speed of catalysis were noted to increase from reference to 2 mL, 4 mL, and 6 mL extract-carrying samples. This happens because size reduction or increase has inverse dependence upon extract concentration, i.e., high concentration of extract decreases particle size or contrarily by lowering concentration increases size and vice versa [67].

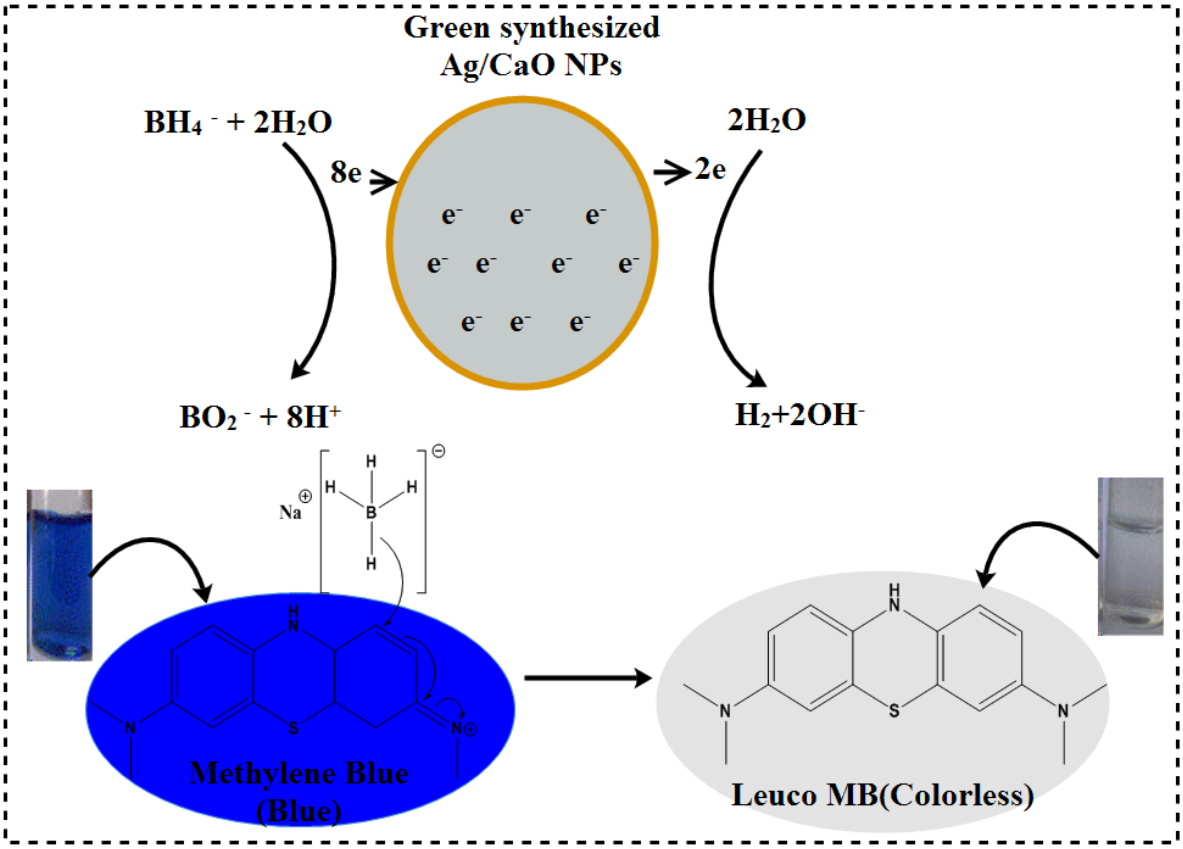

Figure 6 Schematic diagram of catalysis mechanism.

Antimicrobial effectiveness of Ag/CaO containing various concentrations of the extract was obtained from a zone of inhibition (ZOI) measurements through agar well diffusion assay against *S. aureus* (G +ve) and *E. coli* (G –ve) pathogens as shown in Fig. S8 and Table S1. Specific concentrations (0.5 mg/50 µL) and (1.0 mg/50 µL) of un-doped and doped Ag/CaO NCs by extract (2 mL, 4 mL, and 6 mL) were filled into concerning wells and a comparison was conducted with positive control ciprofloxacin (0.005 mg/50 µL) and negative control DI water (50 µL). Results exhibited a strong correlation between ZOI and NCs concentration. Significant (ZOI) ($P < 0.05$) were recorded for all aforementioned samples, ranging (0 – 0.90 mm) and (2.55 – 9.15 mm) for low and high concentrations against *S. aureus*, while (2.60 – 4.70 mm) and (2.95 – 6.30 mm) at low and high concentrations against *E. coli*. The results obtained promised better performance ($P < 0.05$) against both pathogens. Plant extract carries different types of ligands, proteins, tannins, terpenoids, and flavonoids, which interact with microbial membranes [68,69]. Meanwhile, 6 mL sample showed more activity than 4 mL, while 4 mL was better than 2 mL, which was more efficient than the control sample. The most probable justification is that the higher extract concentration possessed a larger number

of ligands, thus rendering better antimicrobial activity. Moreover, it could also be inferred that bacterial vulnerability is enhanced when reducing and capping NCs is achieved [8].

The mechanism is well elaborated where NCs generated intracellular reactive oxygen species (ROS), interact with nucleic acids of the bacterial cell, which encourages singular and dual wrecked break in nitrogenous bases and sugar-phosphate bonds of nucleic acids [70]. It provokes the oxidation of residual amino acids and inactivates key proteins, which consequently disturbs different metabolic processes [71]. Since ROS are toxic toward nucleic acid, thus, probably, it is responsible for DNA breaching of a bacterial cell, as depicted in Fig. S4 [52, 72].

It's crucial to test nanoparticle binding interactions with potential protein targets to better understand molecular and atomic-level events that underpin antibacterial efficacy. The enzyme targets chosen for this study are part of biosynthetic routes, essential for the development or survival of bacteria. A molecular docking analysis was conducted to determine the binding interaction between green synthesized and proteins associated with *E. coli* and *S. aureus*. Ligands were selected from literature as shown in Figure S6 [33, 33]. Best docked complexes were attained for Ag/CaO, ZGN, and SGL (Fig. S5) with DNA gyrase and FabB of *E. coli* and DNA gyrase and DHFR of *S. aureus* (Fig. S5). The docking score was attained for the best-docked configuration of Ag/CaO, ZGN, and SGL with DNA gyrase$_{E.\ coli}$ was 5.00, 10.44, and 8.45, respectively. Ag/CaO formed two hydrogen bonds with key amino acid residue (Asp49 and Asn46). SGL formed H-bonding interactions with Thr165, Arg76, Glu50, Gly 102, and T309. While Gly102, Tyr109, Asn46, and Asp73 are involved in H-bonding within ZGN Fig. 7(a-c). Furthermore, β-keto acyl-[acyl-carrier-protein] synthase (FabB) is an important enzyme in the biosynthesis of fatty acids, and its inhibition can cause bacteria to die. Various studies have reported that thiolactomycin (TLM) and cerulenin (CER) significantly inhibited type II fatty acid synthesis by blocking the activity of FabB (KAS I), which was further confirmed by *in silico* molecular docking analysis [73-76]. In this study, TLM was selected as a reference compound for molecular docking analysis to compare the inhibitory effect of our targeted samples. TLM forms two H-bonds with active site residues (His333 and His298) stabilizing the protein-inhibitor complex. The observed binding score of TLM was 5.56.

The binding score 5.56, 5.52, 8.81, and 6.18 were attained for docking TLM, Ag/CaO, SGL, and ZGN into the active pocket of FabB, respectively. The high binding affinity of SGL

belonging to H-bonding interaction with His333, Gly305, Glu309, and Phe392 in Fig. 7e. These results revealed that synthesized Ag/CaO nanoparticles have a similar binding score compared to TLM, which could be an alternative inhibitor against FabB.

The binding score 5.52, 8.81, and 6.18 was attained for docking of Ag/CaO, SGL, and ZGN into the active pocket of FabB, respectively. The high binding affinity of SGL belonged to H-bonding interaction with T336 and C268, as shown in Fig. 7.

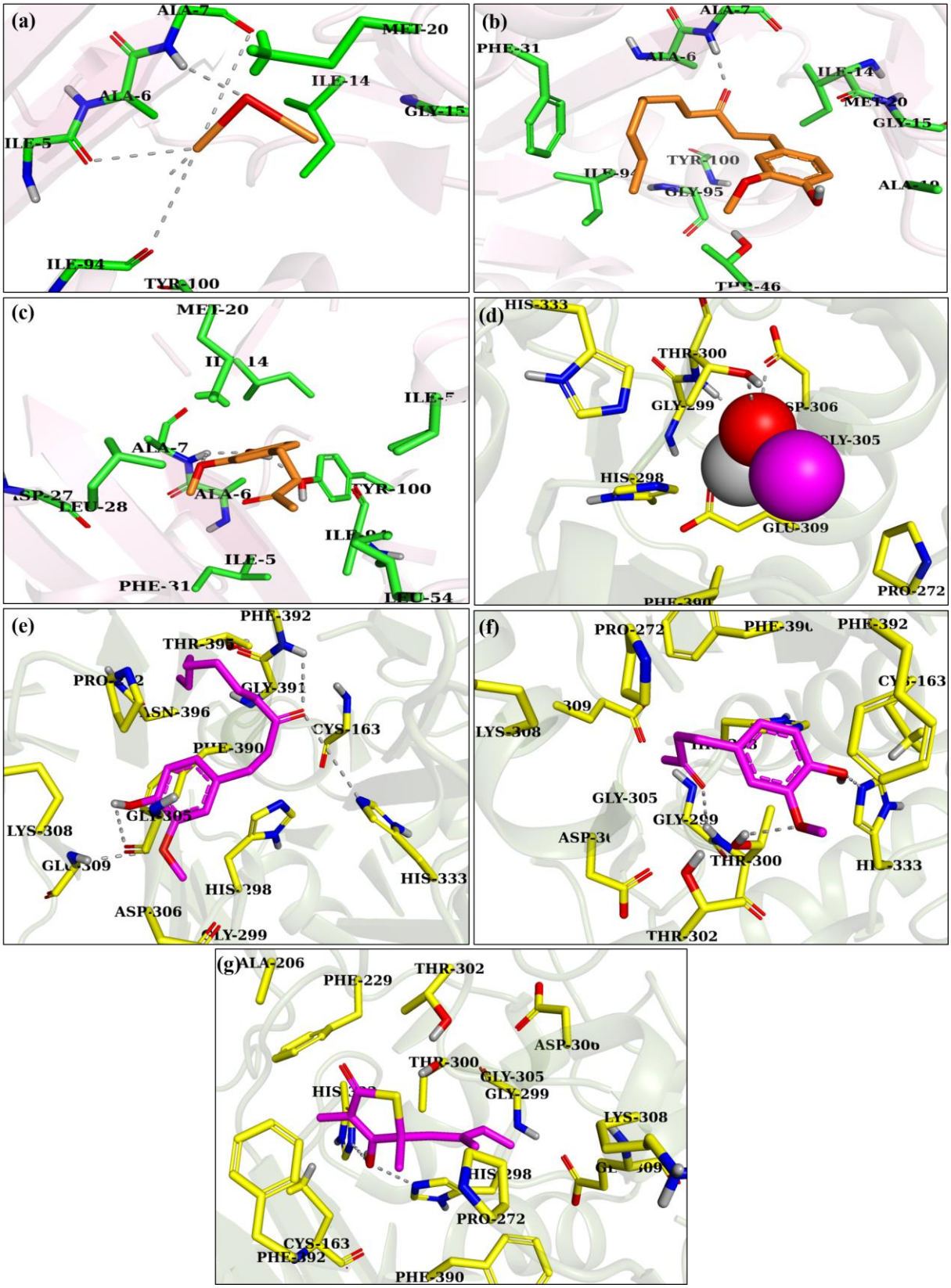

Figure 7 Obtained binding modes of ligands in the binding region of DNA gyrase (salmon) and β-ketoacyl- [acyl carrier protein] synthase I (smudge). (a) Binding of compound Ag/CaO in DNA gyrase binding site. (b) Compound SGL bonded to DNA gyrase. (c) Docking

complex of DNA gyrase-ZGN. Binding mode of selected compounds in active region of β-ketoacyl- [acyl carrier protein] synthase I (FabB): (d) Ag/CaO-FabB, (e) SGL-FabB, (f) ZGN-FabB (g) TLM-FabB from *E. coli* [77, 78].

Similarly, Ag/CaO, SGL, and ZGN binding interaction patterns were evaluated against DHFR from *S. aureus*. The well-docked conformations of Ag/CaO, SGL, and ZGN into an active pocket of DHFR had binding energies of 5.85, 11.26, and 10.10, respectively. T46, L5, and Y98 interacted with Ag/CaO. SGL and ZGN showed H-bonding with S49, T46, Q95, and ZGN showed H-bonding with Q95 and T121 Fig. 8(d-f).

In the instance of DNA gyrase from *S. aureus*, all three ligands (Ag/Cao, SGL, and ZGN) showed H-bonding interaction with G85 with a score of binding 5.24, 8.86, and 8.62, respectively, as shown in Fig. 8 (a-c). The related docking scores are summarized in Table S2. The significant binding score and interaction of the green synthesized Ag/CaO nanoparticles propose them to be a potential inhibitor of dihydrofolate reductase, DNA gyrases, and FabB, which can be investigated further for their enzyme inhibition potential.

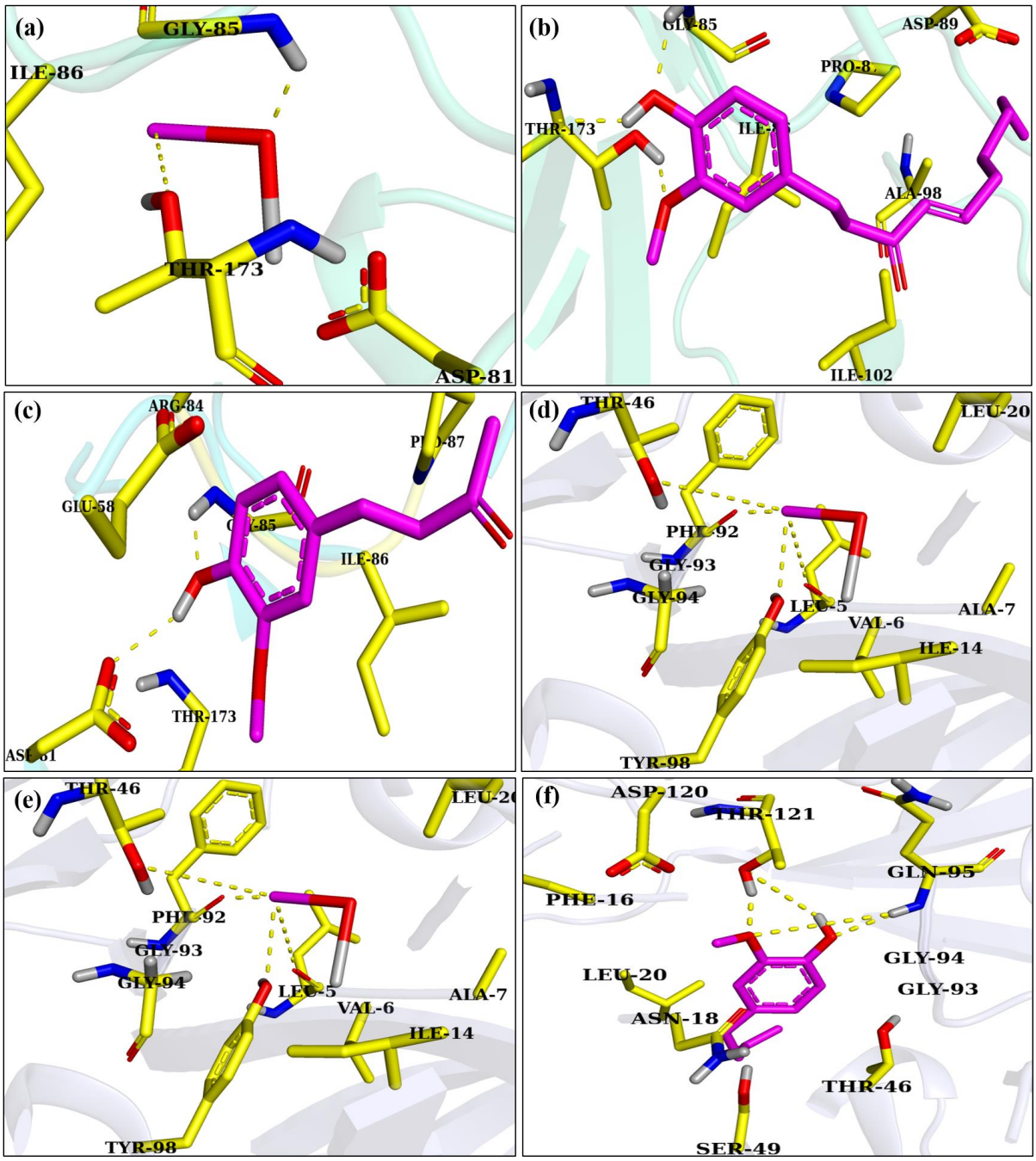

Figure 8 Obtained ligands binding modes in the binding domain of DNA gyrase (light green) and DHFR (light blue). (a) Binding mode of Ag/CaO in the DNA gyrase binding site. (b) Compound SGL bonded with DNA gyrase. (c) Docking complex of DNA gyrase-ZGN. Selected compounds binding mode in the active site of DHFR: (d) Ag/CaO-DHFR, (e) SGL-DHFR, (f) ZGN-DHFR from *S. aureus*.

3. CONCLUSION

CaO and Ag/CaO nanocomposites were synthesized effectively with various extract concentrations using chemical precipitation and green synthesis. The XRD results indicate

that CaO, $CaCO_3$, and $Ca(OH)_2$ possessed an FCC structure and were found in a crystalline condition, with crystallinity increasing with the concentration of doping extract. At 870 and 1440 cm^{-1}, functional groups corresponding to CaO and Ag NPs were observed with FTIR. By doping NCs, a blueshift was seen in UV and PL, resulting in the narrowing of the band gap from 3.25 to 2.93 eV. HRTEM images with lattice fringes revealed an uneven form of Ag and CaO NPs surrounded by a layer of $CaCO_3$ and phytochemicals (0.32-0.28 nm). EDS analysis showed the elemental composition, confirming the presence of Ag, CaO, and other required components for the investigation. The NCs synthesized using biosynthesis exhibited superior antibacterial action against *S. aureus* and *E. coli* compared to those synthesized using chemical precipitation, with the highest activity observed at a 6 mL extract concentration. Catalytic activity measurements of synthesized NCs against MB:CF indicated that NCs synthesized with bio-reduction were much more effective at dye degradation, with activity increasing to the highest level at 6 m L. Additionally, bio-synthesized NCs exhibited increased stability in comparison. In addition, in silico molecular docking studies are in agreement with in vitro bactericidal activity and green synthesized Ag/CaO NCs showed a remarkable binding score and interaction pattern inside the active region of targeted proteins, indicating it may be used as a potential inhibitor of DNA gyrase, DHFR, and FabB enzymes. SGL-containing nanoparticles showed a binding score (8.81) with FabB that is higher than the reference sample TLM (5.56), indicating that it could be an efficient inhibitor as a novel antibiotic agent for bacterial strain. But prior to its use, further research is needed to confirm their inhibition effect by condensing enzyme assay.

ACKNOWLEDGEMENTS

Assistance by the Core Research Facilities at the KFUPM in Dhahran, Saudi Arabia and NRPU (20-17615), HEC Pakistan are deeply appreciated

CONFLICT OF INTEREST

This manuscript is free from any conflict of interest.

REFERENCES

[1] Z. Issaabadi, M. Nasrollahzadeh, S.M. Sajadi, Green synthesis of the copper nanoparticles supported on bentonite and investigation of its catalytic activity, J. Clean. Prod. 142 (2017) 3584–3591. https://doi.org/10.1016/j.jclepro.2016.10.109.

[2] R. Dai, J. Chen, J. Lin, S. Xiao, S. Chen, Y. Deng, Reduction of nitro phenols using

nitroreductase from E. coli in the presence of NADH, J. Hazard. Mater. 170 (2009) 141–143. https://doi.org/10.1016/j.jhazmat.2009.04.122.

[3] M. Ikram, S. Hayat, M. Imran, A. Haider, S. Naz, A. Ul-Hamid, I. Shahzadi, J. Haider, A. Shahzadi, W. Nabgan, S. Ali, Novel Ag/cellulose-doped CeO_2 quantum dots for efficient dye degradation and bactericidal activity with molecular docking study, C. Polymers. 269 (2021)118346. https://doi.org/10.1016/j.carbpol.2021.118346.

[4] P. Wilhelm, D. Stephan, Photodegradation of rhodamine B in aqueous solution via SiO2@TiO2 nano-spheres, J. Photochem. Photobiol. A Chem. 185 (2007) 19–25. https://doi.org/10.1016/j.jphotochem.2006.05.003.

[5] N. Al-Bastaki, Removal of methyl orange dye and Na_2So_4 salt from synthetic waste water using reverse osmosis, Chem. Eng. Process. Process Intensif. 43 (2004) 1561–1567. https://doi.org/10.1016/j.cep.2004.03.001.

[6] N.R. Jana, T. Pal, Growing small metal particle as redox catalyst, Curr. Sci. 75 (1998) 145–149. https://www.jstor.org/stable/24100537

[7] I.K. Sen, K. Maity, S.S. Islam, Green synthesis of gold nanoparticles using a glucan of an edible mushroom and study of catalytic activity, Carbohydr. Polym. 91 (2013) 518–528. https://doi.org/10.1016/j.carbpol.2012.08.058.

[8] S. Munir, A.A. Shah, H. Rahman, M. Bilal, M.S.R. Rajoka, A.A. Khan, M. Khurshid, Nanozymes for medical biotechnology and its potential applications in biosensing and nanotherapeutics, Biotechnol. Lett. 42 (2020) 357–373. https://doi.org/10.1007/s10529-020-02795-3.

[9] A. Javaid, S. Latif, M. Imran, N. Hussain, M.S.R. Rajoka, H.M.N. Iqbal, M. Bilal, Nanohybrids-assisted photocatalytic removal of pharmaceutical pollutants to abate their toxicological effects – A review, Chemosphere. 291 (2022) 133056. https://doi.org/10.1016/j.chemosphere.2021.133056.

[10] C. Vijilvani, M.R. Bindhu, F.C. Frincy, M.S. AlSalhi, S. Sabitha, K. Saravanakumar, S. Devanesan, M. Umadevi, M.J. Aljaafreh, M. Atif, Antimicrobial and catalytic activities of biosynthesized gold, silver and palladium nanoparticles from Solanum nigurum leaves, J. Photochem. Photobiol. B Biol. 202 (2020) 111713. https://doi.org/10.1016/j.jphotobiol.2019.111713.

[11] Elgorashi, Esameldin E., Joslyn LS Taylor, Annemarie Maes, Johannes van Staden, Norbert De Kimpe, and Luc Verschaeve. "Screening of medicinal plants used in South African traditional medicine for genotoxic effects." *Toxicology letters* 143, no. 2 (2003): 195-207.

[12] S. Komarneni, D. Li, B. Newalkar, H. Katsuki, A.S. Bhalla, Microwave - Polyol process for Pt and Ag nanoparticles, Langmuir. 18 (2002) 5959–5962. https://doi.org/10.1021/la025741n.

[13] R. Jose Varghese, N. Zikalala, E.H.M. Sakho, O.S. Oluwafemi, Green synthesis protocol on metal oxide nanoparticles using plant extracts, Elsevier Inc., (2020) 67-82. https://doi.org/10.1016/b978-0-12-813357-6.00006-1.

[14] J.G. Parsons, J.R. Peralta-Videa, J.L. Gardea-Torresdey, Use of plants in biotechnology: Synthesis of metal nanoparticles by inactivated plant tissues, plant extracts, and living plants, Dev. Environ. Sci. 5 (2007) 463–485. https://doi.org/10.1016/S1474-8177(07)05021-8.

[15] J. M. Chem, J. Lee, H. Y. Kim, H. Zhou, S. Hwang, K. Koh, D. Han, J. Lee, Green synthesis of phytochemical-stabilized Au nanoparticles under ambient conditions and their biocompatibility and antioxidative activity †, (2011) 13316–13326. https://doi.org/10.1039/c1jm11592h.

[16] M.N. Nadagouda, R.S. Varma, Green synthesis of silver and palladium nanoparticles at room temperature using coffee and tea extract, Green Chem. 10 (2008) 859–86. https://doi.org/10.1039/b804703k.

[17] M. N. Nadagouda, R. S. Varma, Green synthesis of silver and palladium nanoparticles at room temperature using coffee and tea extract, (2008) 859–862. https://doi.org/10.1039/b804703k.

[18] L. Wang, C. Hu, L. Shao, The antimicrobialactivity of nanoparticles present situatiation and prospects for the future, Int. J. Nanomedicine. 12 (2017) 1227–1249. https://www.ncbi.nlm.nih.gov/pmc/articles/PMC5317269/pdf/ijn-12-1227.pdf.

[19] B. Ramola, N.C. Joshi, Green Synthesis, Characterisations and Antimicrobial Activities of CaO Nanoparticles, Orient. J. Chem. 35 (2019) 1154–1157. https://doi.org/10.13005/ojc/350333.

[20] K.J. Woo, C.K. Hye, W.K. Ki, S. Shin, H.K. So, H.P. Yong, Antibacterial activity and mechanism of action of the silver ion in Staphylococcus aureus and Escherichia coli, Appl. Environ. Microbiol. 74 (2008) 2171–2178. https://doi.org/10.1128/AEM.02001-07.

[21] X. Wang, Y. Du, L. Fan, H. Liu, Y. Hu, Chitosan- metal complexes as antimicrobial agent: Synthesis, characterization and Structure-activity study, Polym. Bull. 55 (2005) 105–113. https://doi.org/10.1007/s00289-005-0414-1.

[22] S. Pal, E.J. Yoon, Y.K. Tak, E.C. Choi, J.M. Song, Synthesis of highly antibacterial nanocrystalline trivalent silver polydiguanide, Chem. Soc. 131 (2009) 16147–16155. https://doi.org/10.1021/ja9051125.

[23] L. Huang, H. Yang, Y. Zhang, W. Xiao, Study on Synthesis and Antibacterial Properties of Ag NPs/GO Nanocomposites, J. Nanomater. 2016 (2016). https://doi.org/10.1155/2016/5685967.

[24] I. Jahan, F. Erci, R. Cakir-Koc, I. Isildak, Microwave-irradiated green synthesis of metallic silver and copper nanoparticles using fresh ginger (Zingiber officinale) rhizome extract and evaluation of their antibacterial potentials and cytotoxicity, Inorg. Nano-Metal Chem. 51 (2020) 722–732. https://doi.org/10.1080/24701556.2020.1808017.

[25] S. Prasad, A.K. Tyagi, Ginger and its constituents: Role in prevention and treatment of gastrointestinal cancer, Gastroenterol. Res. Pract. 2015 (2015). https://doi.org/10.1155/2015/142979.

[26] I. Khan, A. Mazumdar, S. Pathak, P. Paul, S. Kumar, A.J. Tamhankar, S.K. Tripathy, C. Stalsby, A. Mishra, Biointerfaces Biogenic Ag/CaO nanocomposites kill Staphylococcus aureus with reduced toxicity towards mammalian cells, Colloids Surfaces B Biointerfaces. 189 (2020) 110846. https://doi.org/10.1016/j.colsurfb.2020.110846.

[27] G. Kania, M. Nowakowska, Hybrid calcium carbonate / polymer microparticles containing silver nanoparticles as antibacterial agents, (2012). https://doi.org/10.1007/s11051-012-1313-7.

[28] D. Paul, D. Sachan, G. Das, Silver nanoparticles embedded on in-vitro biomineralized

vaterite : A highly efficient catalyst with enhanced catalytic activity towards 4-Nitrophenol reduction, Mol. Catal. 504 (2021) 111433. https://doi.org/10.1016/j.mcat.2021.111433.

[29] A. Haider, M. Ijaz, M. Imran, M. Naz, H. Majeed, J.A. Khan, M.M. Ali, M. Ikram, Enhanced bactericidal action and dye degradation of spicy roots' extract-incorporated fine-tuned metal oxide nanoparticles, Appl. Nanosci. 10 (2020) 1095–1104. https://doi.org/10.1007/s13204-019-01188-x.

[30] H. Abdul Salam, R. Sivaraj, R. Venckatesh, Green synthesis and characterization of zinc oxide nanoparticles from Ocimum basilicum L. var. purpurascens Benth.-Lamiaceae leaf extract, Mater. Lett. 131 (2014) 16–18. https://doi.org/10.1016/j.matlet.2014.05.033.

[31] A. Haider, M. Ijaz, M. Imran, M. Naz, M. Majeed, J.A Khan, M. Ikram, Enhanced bactericidal action and dye degradation of spicy roots ' extract ‐ incorporated fine ‐ tuned metal oxide nanoparticles, A.Science. 10 (2021) 1095-1104.

[32] J.R. Manjunatha, B.K. Bettadaiah, P.S. Negi, P. Srinivas, Synthesis of quinoline derivatives of tetrahydrocurcumin and zingerone and evaluation of their antioxidant and antibacterial attributes, Food Chem. 136 (2013) 650–658. https://doi.org/10.1016/j.foodchem.2012.08.052.

[33] S. Rampogu, A. Baek, R.G. Gajula, A. Zeb, R.S. Bavi, R. Kumar, Y. Kim, Y.J. Kwon, K.W. Lee, Ginger (Zingiber officinale) phytochemicals-gingerenone-A and shogaol inhibit SaHPPK: Molecular docking, molecular dynamics simulations and in vitro approaches, Ann. Clin. Microbiol. Antimicrob. 17 (2018) 1–15. https://doi.org/10.1186/s12941-018-0266-9.

[34] L.S. Nelson, K.Y. Lee, C.R. Kumana, β-Lactam Antibiotic and β- Lactamase Inhibitor Combinations, Nursing (Lond). 285 (2001) 2–4. https://doi:10.1001/jama.285.4.386

[35] H.Q. Li, L. Shi, Q.S. Li, P.G. Liu, Y. Luo, J. Zhao, H.L. Zhu, Synthesis of C(7) modified chrysin derivatives designing to inhibit $β$-ketoacyl-acyl carrier protein synthase III (FabH) as antibiotics, Bioorganic Med. Chem. 17 (2009) 6264–6269. https://doi.org/10.1016/j.bmc.2009.07.046.

[36] S. Naz, T. Ngo, U. Farooq, R. Abagyan, Analysis of drug binding pockets and

repurposing opportunities for twelve essential enzymes of ESKAPE pathogens, PeerJ. 2017 (2017) 1–16. https://doi.org/10.7717/peerj.3765.

[37] M.F. Mesleh, J.B. Cross, J. Zhang, J. Kahmann, O.A. Andersen, J. Barker, R.K. Cheng, B. Felicetti, M. Wood, A.T. Hadfield, C. Scheich, T.I. Moy, Q. Yang, J. Shotwell, K. Nguyen, B. Lippa, R. Dolle, M.D. Ryan, Fragment-based discovery of DNA gyrase inhibitors targeting the ATPase subunit of GyrB, Bioorganic Med. Chem. Lett. 26 (2016) 1314–1318. https://doi.org/10.1016/j.bmcl.2016.01.009.

[38] C. Oefner, S. Parisi, H. Schulz, S. Lociuro, G.E. Dale, Inhibitory properties and X-ray crystallographic study of the binding of AR-101, AR-102 and iclaprim in ternary complexes with NADPH and dihydrofolate reductase from Staphylococcus aureus, Acta Crystallogr. Sect. D Biol. Crystallogr. 65 (2009) 751–757. https://doi.org/10.1107/S0907444909013936.

[39] F. V Stanger, C. Dehio, T. Schirmer, Structure of the N-Terminal Gyrase B fragment in complex with ADP?Pi reveals rigid-body motion induced by ATP hydrolysis, PLoS One. 9 (2014). https://doi.org/10.1371/journal.pone.0107289.

[40] A.C. Price, K.H. Choi, R.J. Heath, Z. Li, S.W. White, C.O. Rock, Inhibition of $β$-ketoacyl-acyl carrier protein synthases by thiolactomycin and cerulenin: Structure and mechanism, J. Biol. Chem. 276 (2001) 6551–6559. https://doi.org/10.1074/jbc.M007101200.

[41] K. Rehman, T.A. Chohan, I. Waheed, Z. Gilani, M.S.H. Akash, Taxifolin prevents postprandial hyperglycemia by regulating the activity of $α$-amylase: Evidence from an in vivo and in silico studies, J. Cell. Biochem. 120 (2019) 425–438. https://doi.org/10.1002/jcb.27398.

[42] A.N. Jain, Surflex: Fully automatic flexible molecular docking using a molecular similarity-based search engine, J. Med. Chem. 46 (2003) 499–511. https://doi.org/10.1021/jm020406h.

[43] M. Clark, R.D. Cramer, N. Van Opdenbosch, Validation of the general purpose tripos 5.2 force field, J. Comput. Chem. 10 (1989) 982–1012. https://doi.org/10.1002/jcc.540100804.

[44] W. Welch, J. Ruppert, A.N. Jain, Hammerhead: Fast, fully automated docking of

flexible ligands to protein binding sites, Chem. Biol. 3 (1996) 449–462. https://doi.org/10.1016/S1074-5521(96)90093-9.

[45] A.N. Jain, Scoring noncovalent protein-ligand interactions: A continuous differentiable function tuned to compute binding affinities, J. Comput. Aided. Mol. Des. 10 (1996) 427–440. https://doi.org/10.1007/BF00124474.

[46] F.S. Kodeh, I.M. Nahhal, N. Emad, A. Elkhair, A.H. Darwish, Synthesis of CaO–Ag NPs @ $CaCO_3$ Nanocomposite via Impregnation of Aqueous Sol Ag NPs onto Calcined Calcium Oxalate, Chem. Africa. (2019). https://doi.org/10.1007/s42250-019-00112-8.

[47] V. Apalangya, V. Rangari, B. Tiimob, S. Jeelani, T. Samuel, Applied Surface Science Development of antimicrobial water filtration hybrid material from bio source calcium carbonate and silver nanoparticles, Appl. Surf. Sci. 295 (2014) 108–114. https://doi.org/10.1016/j.apsusc.2014.01.012.

[48] A. Haider, M. Ijaz, S. Ali, J. Haider, M. Imran, H. Majeed, I. Shahzadi, M.M. Ali, J.A. Khan, M. Ikram, Green Synthesized Phytochemically (Zingiber officinale and Allium sativum) Reduced Nickel Oxide Nanoparticles Confirmed Bactericidal and Catalytic Potential, 50 (2020).

[49] M.C. Tsiaganis, K. Laskari, E. Melissari, Fatty acid composition of Allium species lipids, 19 (2006) 620–627. https://doi.org/10.1016/j.jfca.2005.06.003.

[50] V.P. Sarathy, Research Article Biomedical Applications of Calcium Oxide Nanoparticles - A Spectroscopic Study, 49 (2018) 121–125.

[51] J. Yoonus, R. Resmi, B. Beena, Materials Today : Proceedings Greener nanoscience : Piper betel leaf extract mediated synthesis of CaO nanoparticles and evaluation of its antibacterial and anticancer activity, Mater. Today Proc. (2020). https://doi.org/10.1016/j.matpr.2020.05.246.

[52] I. Khan, A. Mazumdar, S. Pathak, P. Paul, S. Kumar, A.J. Tamhankar, K. Saraj, Tripathy, C. Stalsby, A. Mishra, Biogenic Ag / CaO nanocomposites kill Staphylococcus aureus with reduced toxicity towards mammalian cells, Colloids Surfaces B Biointerfaces. 189 (2020) 110846. https://doi.org/10.1016/j.colsurfb.2020.110846.

[53] A. Haider, M. Ijaz, M. Imran, M. Naz, H. Majeed, J.A. Khan, M.M. Ali, M. Ikram, Enhanced bactericidal action and dye degradation of spicy roots' extract-incorporated fine-tuned metal oxide nanoparticles, Appl. Nanosci. 10 (2020) 1095–1104. https://doi.org/10.1007/s13204-019-01188-x.

[54] A. Haider, M. Ijaz, S. Ali, J. Haider, M. Imran, H. Majeed, I. Shahzadi, M.M. Ali, J.A. Khan, M. Ikram, Green Synthesized Phytochemically (Zingiber officinale and Allium sativum) Reduced Nickel Oxide Nanoparticles Confirmed Bactericidal and Catalytic Potential, Nanoscale Res. Lett. 15 (2020). https://doi.org/10.1186/s11671-020-3283-5.

[55] T.C. Prathna, N. Chandrasekaran, A.M. Raichur, A. Mukherjee, Colloids and Surfaces B : Biointerfaces Biomimetic synthesis of silver nanoparticles by Citrus limon (lemon) aqueous extract and theoretical prediction of particle size, Colloids Surfaces B Biointerfaces. 82 (2011) 152–159. https://doi.org/10.1016/j.colsurfb.2010.08.036.

[56] A. Henglein, Physicochemical properties of small metal particles in solution: "Microelectrode" reactions, chemisorption, composite metal particles, and the atom-to-metal transition, J. Phys. Chem. 97 (1993) 5457–5471. https://doi.org/10.1021/j100123a004.

[57] S. Bano, S. Pillai, Green synthesis of calcium oxide nanoparticles at different calcination temperatures, World J. Sci. Technol. Sustain. Dev. 17 (2020) 283–295. https://doi.org/10.1108/wjstsd-12-2019-0087.

[58] T. V Shahbazyan, I.E. Perakis, J.Y. Bigot, Size-dependent surface plasmon dynamics in metal nanoparticles, Phys. Rev. Lett. 81 (1998) 3120–3123. https://doi.org/10.1103/PhysRevLett.81.3120.

[59] V. Kravets, Z. Almemar, K. Jiang, K. Culhane, R. Machado, G. Hagen, A. Kotko, I. Dmytruk, K. Spendier, A. Pinchuk, Imaging of biological cells using luminescent silver nanoparticles, Nanoscale Res. Lett. 11 (2016). https://doi.org/10.1186/s11671-016-1243-x.

[60] E. Dulkeith, T. Niedereichholz, T.A. Klar, J. Feldmann, G. Von Plessen, D.I. Gittins, K.S. Mayya, F. Caruso, Plasmon emission in photoexcited gold nanoparticles, Phys. Rev. B - Condens. Matter Mater. Phys. 70 (2004) 1–4. https://doi.org/10.1103/PhysRevB.70.205424.

[61] S. Sood, A. Umar, S.K. Mehta, S.K. Kansal, Highly effective Fe-doped TiO_2 nanoparticles photocatalysts for visible-light driven photocatalytic degradation of toxic organic compounds, J. Colloid Interface Sci. 450 (2015) 213–223. https://doi.org/10.1016/j.jcis.2015.03.018.

[62] J. Zhu, W. Zheng, B. He, J. Zhang, M. Anpo, Characterization of Fe-TiO_2 photocatalysts synthesized by hydrothermal method and their photocatalytic reactivity for photodegradation of XRG dye diluted in water, J. Mol. Catal. A Chem. 216 (2004) 35–43. https://doi.org/10.1016/j.molcata.2004.01.008.

[63] G. Rajakumar, M. Thiruvengadam, G. Mydhili, T. Gomathi, I.M. Chung, Green approach for synthesis of zinc oxide nanoparticles from Andrographis paniculata leaf extract and evaluation of their antioxidant, anti-diabetic, and anti-inflammatory activities, Bioprocess Biosyst. Eng. 41 (2018) 21–30. https://doi.org/10.1007/s00449-017-1840-9.

[64] M. Ali, M. Ikram, M. Ijaz, A. Ul-Hamid, M. Avais, A.A. Anjum, Green synthesis and evaluation of n-type ZnO nanoparticles doped with plant extract for use as alternative antibacterials, Appl. Nanosci. 10 (2020) 3787–3803. https://doi.org/10.1007/s13204-020-01451-6.

[65] S. Chandra Paul, S. Bhowmik, M. Rani Nath, M.S. Islam, S. Kanti Paul, J. Neazi, T. Sabnam Binta Monir, S. Dewanjee, M. Abdus Salam, Silver Nanoparticles Synthesis in a Green Approach: Size Dependent Catalytic Degradation of Cationic and Anionic Dyes, Orient. J. Chem. 36 (2020) 353–360. https://doi.org/10.13005/ojc/360301.

[66] A. Sahoo, S. Patra, A Combined Process for the Degradation of Azo-Dyes and Efficient Removal of Aromatic Amines Using Porous Silicon Supported Porous Ruthenium Nanocatalyst, ACS Appl. Nano Mater. 1 (2018) 5169–5178. https://doi.org/10.1021/acsanm.8b01152.

[67] D.T. Handago, E.A. Zereffa, B.A. Gonfa, Effects of Azadirachta Indica Leaf Extract, Capping Agents, on the Synthesis of Pure and Cu Doped ZnO-Nanoparticles: A Green Approach and Microbial Activity, Open Chem. 17 (2019) 246–253. https://doi.org/10.1515/chem-2019-0018.

[68] M. Reda, A. Ashames, Z. Edis, S. Bloukh, R. Bhandare, H.A. Sara, Green synthesis of

potent antimicrobial silver nanoparticles using different plant extracts and their mixtures, Processes. 7 (2019). https://doi.org/10.3390/pr7080510.

[69] N.J. Reddy, D. Nagoor Vali, M. Rani, S.S. Rani, Evaluation of antioxidant, antibacterial and cytotoxic effects of green synthesized silver nanoparticles by Piper longum fruit, Mater. Sci. Eng. C. 34 (2014) 115–122. https://doi.org/10.1016/j.msec.2013.08.039.

[70] M. Nita, A. Grzybowski, The Role of the Reactive Oxygen Species and Oxidative Stress in the Pathomechanism of the Age-Related Ocular Diseases and Other Pathologies of the Anterior and Posterior Eye Segments in Adults, Oxid. Med. Cell. Longev. 2016 (2016). https://doi.org/10.1155/2016/3164734.

[71] H. Cui, Y. Kong, H. Zhang, Oxidative Stress, Mitochondrial Dysfunction, and Aging, J. Signal Transduct. 2012 (2012) 1–13. https://doi.org/10.1155/2012/646354.

[72] M.D. Evans, M. Dizdaroglu, M.S. Cooke, Oxidative DNA damage and disease: Induction, repair and significance, 2004. https://doi.org/10.1016/j.mrrev.2003.11.001.

[73] Jackowski, S., Zhang, Y.M., Price, A.C., White, S.W. and Rock, C.O., 2002. A missense mutation in the fabB (β-ketoacyl-acyl carrier protein synthase I) gene confers thiolactomycin resistance to Escherichia coli. *Antimicrobial agents and chemotherapy*, *46*(5), pp.1246-1252.

[74] Price, A.C. and Choi, K.H., RJ Health, Z. Li, SW White, and CO Rock. 2001. Inhibition of β-ketoacyl-[acyl carrier protein] synthases by thiolactomycin and cerulenin: structure and mechanism. *J. Biol. Chem*, *276*, pp.6551-6559.

[75] Pappenberger, G., Schulz-Gasch, T., Kusznir, E., Müller, F. and Hennig, M., 2007. Structure-assisted discovery of an aminothiazole derivative as a lead molecule for inhibition of bacterial fatty-acid synthesis. *Acta Crystallographica Section D: Biological Crystallography*, *63*(12), pp.1208-1216.

[76] Sabbagh, G. and Berakdar, N., 2015. Docking studies of flavonoid compounds as inhibitors of β-ketoacyl acyl carrier protein synthase I (Kas I) of Escherichia coli. *Journal of Molecular Graphics and Modelling*, *61*, pp.214-223.

[77] M.S. Riaz Rajoka, H.M. Mehwish, H. Zhang, M. Ashraf, H. Fang, X. Zeng, Y. Wu, M.

Khurshid, L. Zhao, Z. He, Antibacterial and antioxidant activity of exopolysaccharide mediated silver nanoparticle synthesized by Lactobacillus brevis isolated from Chinese koumiss, Colloids Surfaces B Biointerfaces. 186 (2020) 110734. https://doi.org/10.1016/j.colsurfb.2019.110734.

[78] H.M. Mehwish, G. Liu, M.S.R. Rajoka, H. Cai, J. Zhong, X. Song, L. Xia, M. Wang, R.M. Aadil, M. Inam-Ur-Raheem, Y. Xiong, H. Wu, M.I. Amirzada, Q. Zhu, Z. He, Therapeutic potential of Moringa oleifera seed polysaccharide embedded silver nanoparticles in wound healing, Int. J. Biol. Macromol. 184 (2021) 144–158. https://doi.org/10.1016/j.ijbiomac.2021.05.202.

SUPPLEMENTARY MATERIALS

Z. Officinale-Doped Silver/Calcium Oxide Nanocomposites: Catalytic Activity and Antimicrobial Potential with Molecular Docking Analysis

Zakariya Mehmood[a], Muhammad Ikram[a*], Muhammad Imran[b], Anum Shahzadi[c], Ali Haider[d], Anwar Ul-Hamid[e*], Walid Nabgan[f*], Junaid Haider[g], Shaukat Hayat[h]

[a]Solar Cell Application Research Lab, Department of Physics, Government College University Lahore, Lahore, 54000, Punjab, Pakistan

[b]State key Laboratory of Chemical Resource Engineering, Beijing Advanced Innovation Centre for Soft Matter Science and Engineering, Beijing Engineering Centre for Hierarchical Catalysts, Beijing University of Chemical Technology, Beijing 100029, China

[c]Faculty of Pharmacy, The University of Lahore, 54000, Lahore, Pakistan

[d]Department of Clinical Sciences, Faculty of Veterinary and Animal Sciences, Muhammad Nawaz Shareef, University of Agriculture, Multan, 66000, Punjab, Pakistan

[e]Core Research Facilities, King Fahd University of Petroleum & Minerals, Dhahran, 31261, Saudi Arabia

[f]School of Chemical and Energy Engineering, Faculty of Engineering, Universiti Teknologi Malaysia, 81310, Skudai, Johor, Malaysia

[g]Tianjin Institute of Industrial Biotechnology, Chinese Academy of Sciences, Tianjin 300308, China.

[h]Department of Physics, Riphah Institute of Computing and Applied Sciences (RICAS), Riphah International University, 14 Ali Road, Lahore, Pakistan

*Corresponding authors emails: [a]dr.muhammadikram@gcu.edu.pk, [e]anwar@kfupm.edu.sa, [f]wnabgan@gmail.com

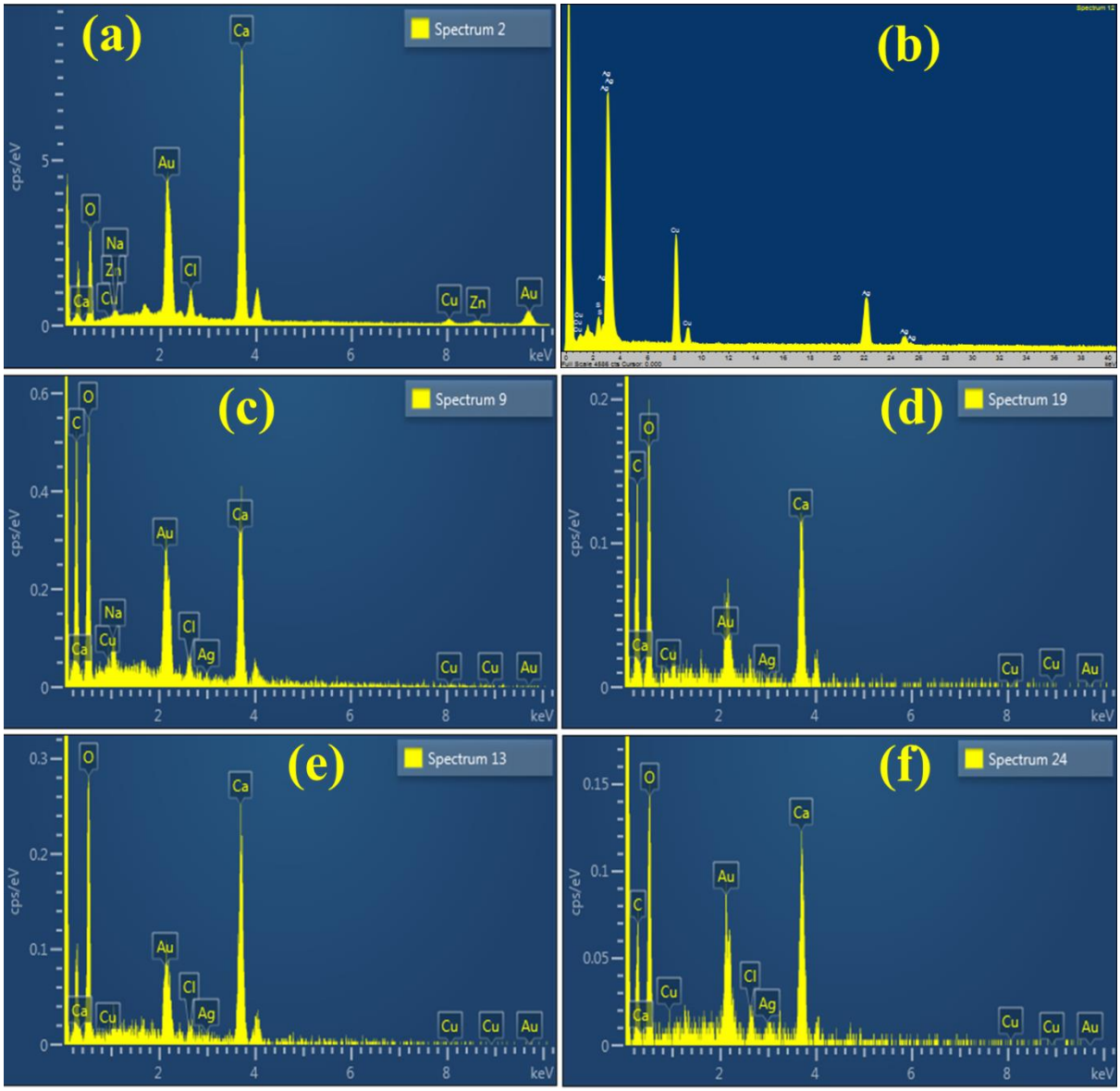

Figure S1 EDS analysis of (a) CaO, (b) Ag, (c) Ag/CaO, and (d-f) (2, 4 and 6 mL) extract doped Ag/CaO NCs, respectively.

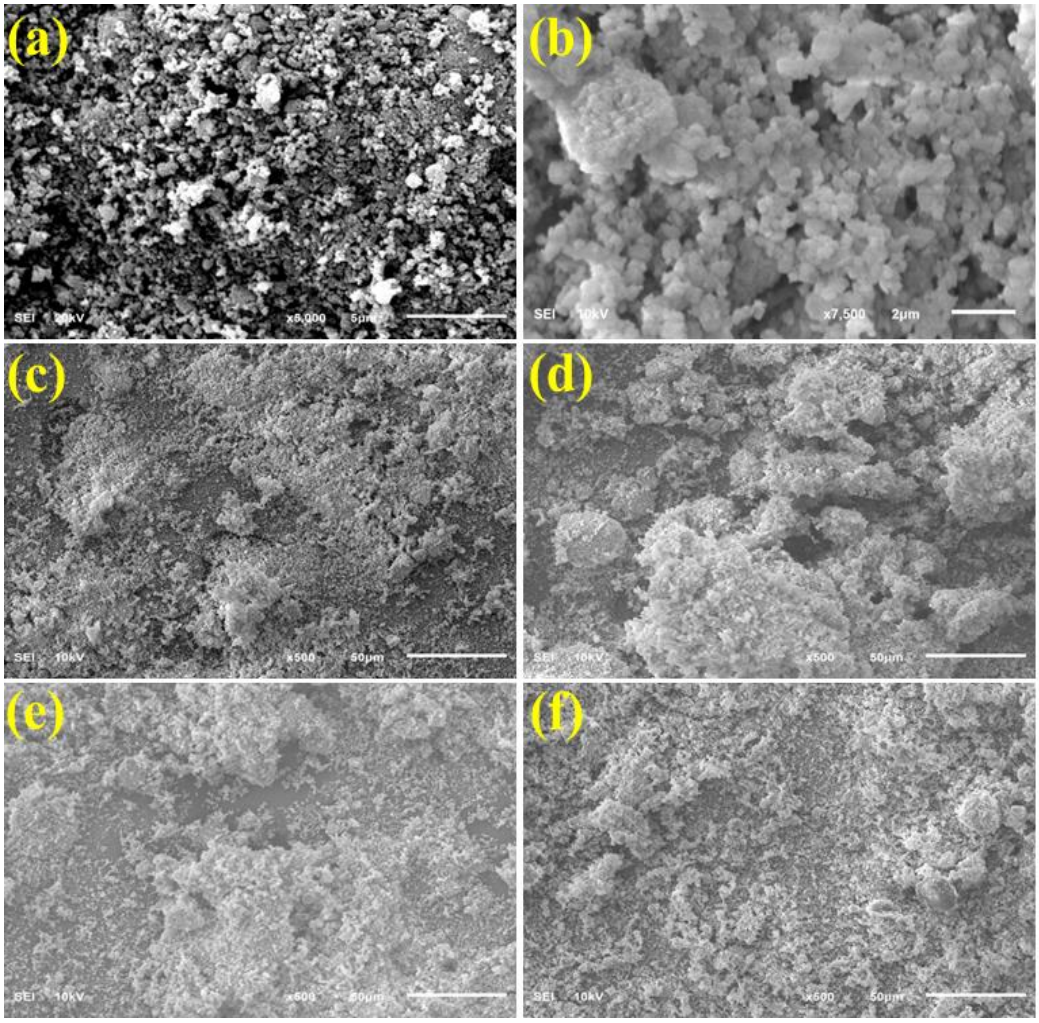

Figure S2 (a-f) FE-SEM micro images of pure CaO, Ag, Ag/CaO, and 2 mL, 4 mL and 6 mL extract doped Ag/CaO NCs, respectively.

The morphology of CaO, Ag, and with 2, 4, and 6 mL extract-doped Ag/CaO NCs was analyzed using FE-SEM as shown in S2. The images showed NCs to be spherical, agglomerated and clamped to each other. The supersaturated nature of the trigonas*p* honey may explain such agglomerated and clamped structure. The agglomeration occurs due to the fusion of smaller particles during synthesis.

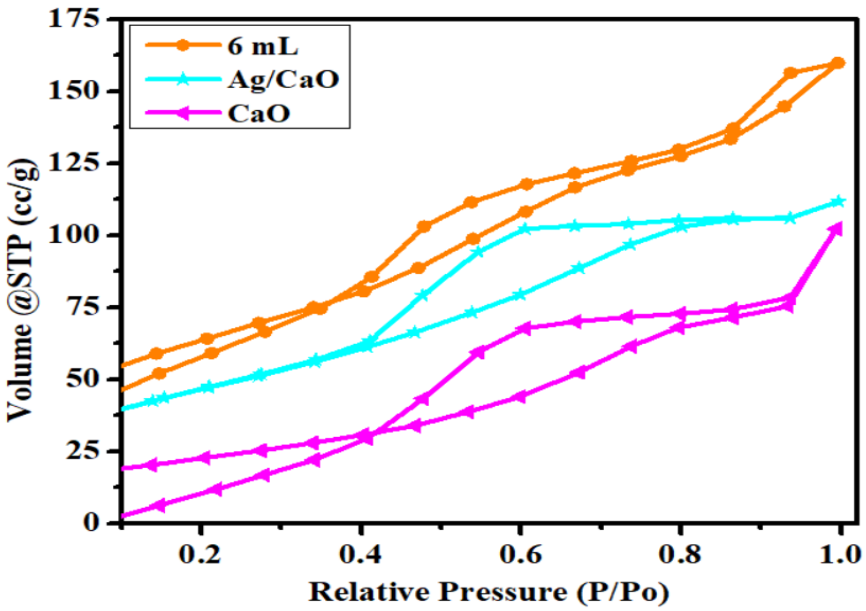

Figure S3: N_2 Adsorption/desorption isotherm of CaO, Ag/CaO, and 6 mL extract-doped Ag/CaO nanocomposites

Fig. S3 shows N_2 adsorption/desorption isotherms of CaO, Ag/CaO, and 6 mL extract-doped Ag/CaO nanocomposites, respectively, used to investigate BET surface areas. All of the concerned samples displayed the typical type IV isotherms with distinct H_2 type hysteresis loop ranging from 0.4-1.0 at relatively high-pressure P/P_0, which indicated the existence of well-developed mesoporous structure [1,2]. Consequently, it was observed that 6 mL extract-doped, Ag/CaO, and CaO had estimated BET surface area of 157.95, 111.73, and 102.24 $m^2g^{-1,}$ respectively. BET surface areas of 6 mL extract-doped Ag/CaO NCs increased with incorporating Ag and extracted dopant. An increase in surface areas is thought to provide more active sites; enable easy charge-carrier transport and result in enhanced photocatalytic performance [3,4].

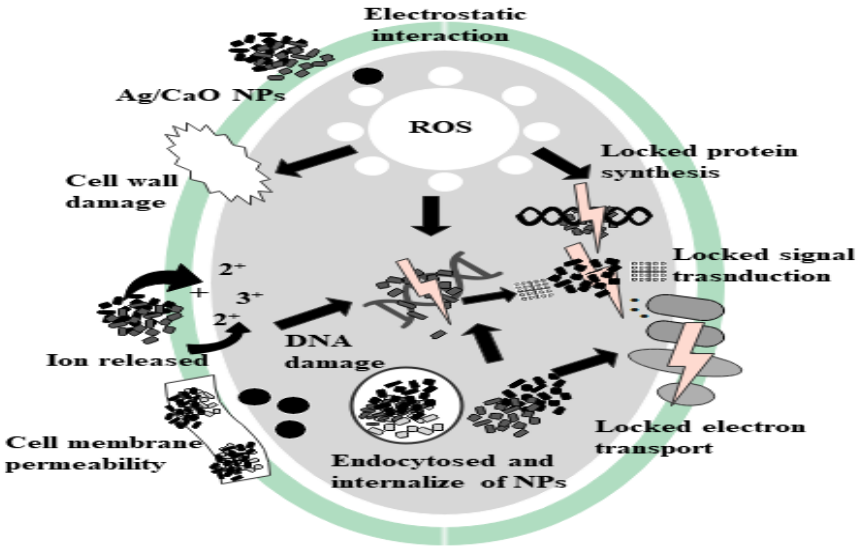

Figure S4 Schematic diagram of antimicrobial mechanism.

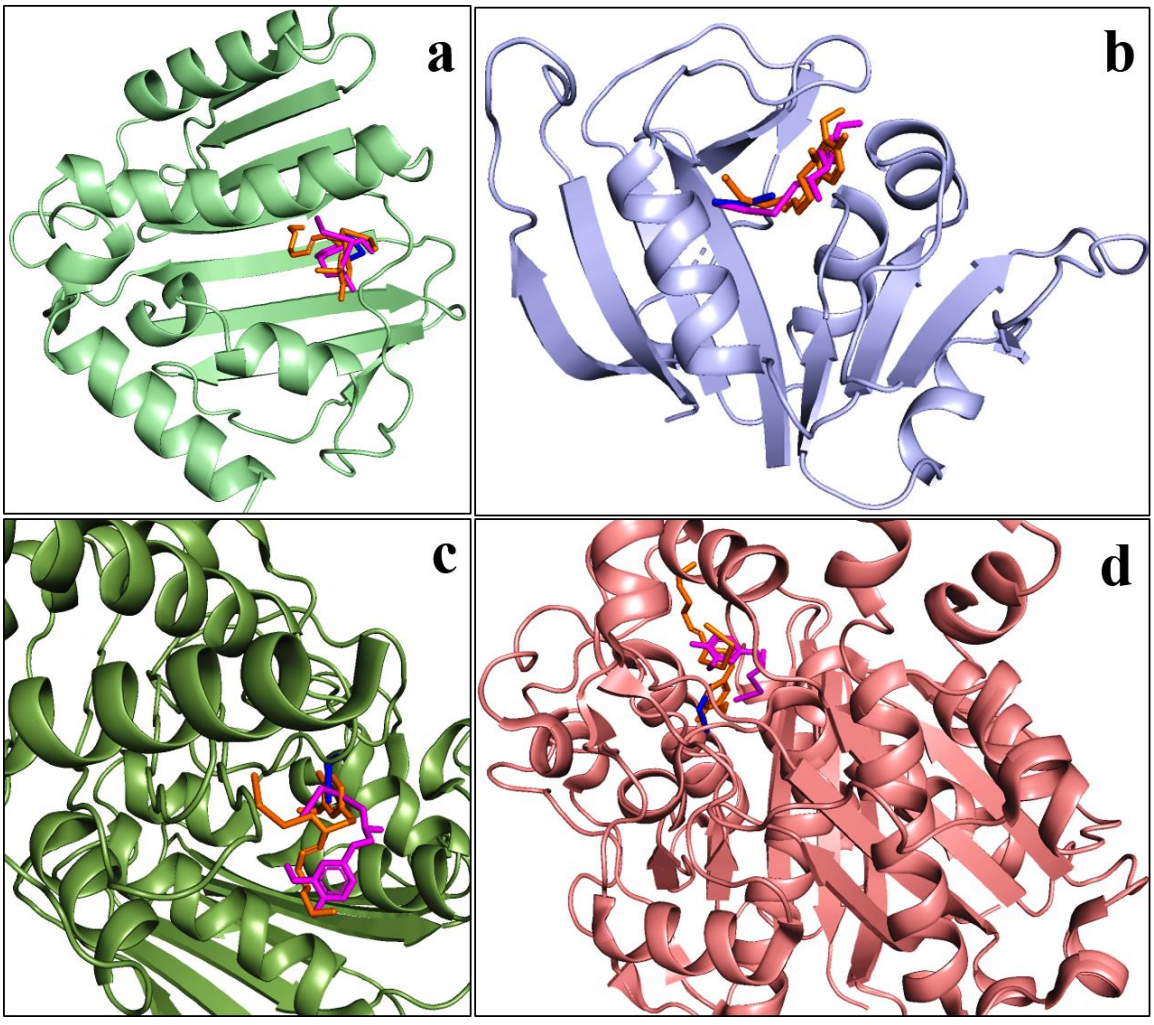

Figure S5. Obtained binding mode of ligands in the domain of targeted protein (a) Ag/CaO-, SGL- and ZGN-DNA gyrase*S. aureus* (b) Ag/CaO-, SGL- and ZGN- DHFR of *S. aureus* (c) Ag/CaO-, SGL- and ZGN- FabB (d) Ag/CaO-, SGL- and ZGN-DNA gyrase*E. coli*

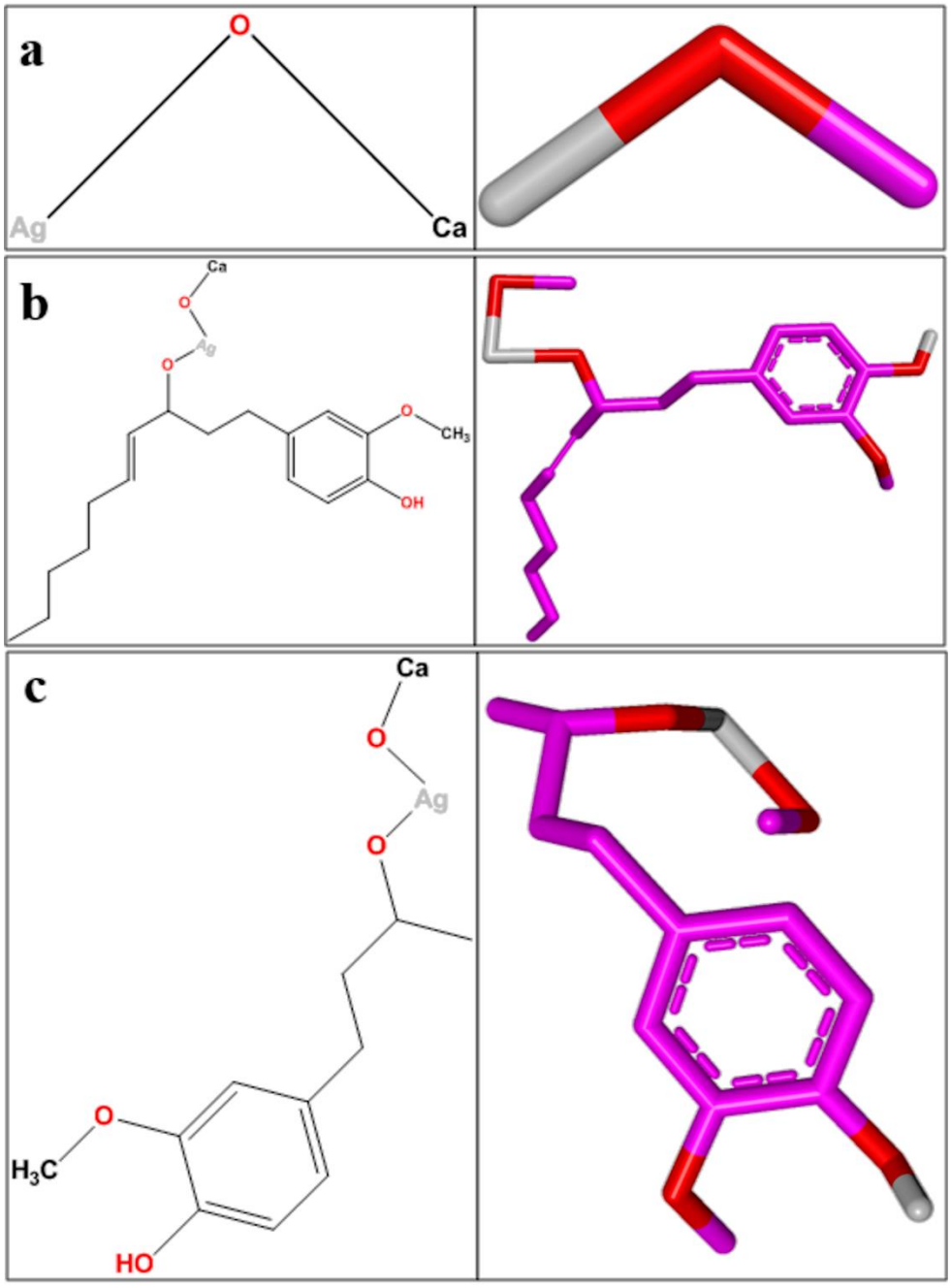

Figure S6. Chemical structures in 2D and 3D view (a) Ag/CaO (b) shagoal bonded to Ag/Cao (c) zingerone bonded to Ag/CaO.

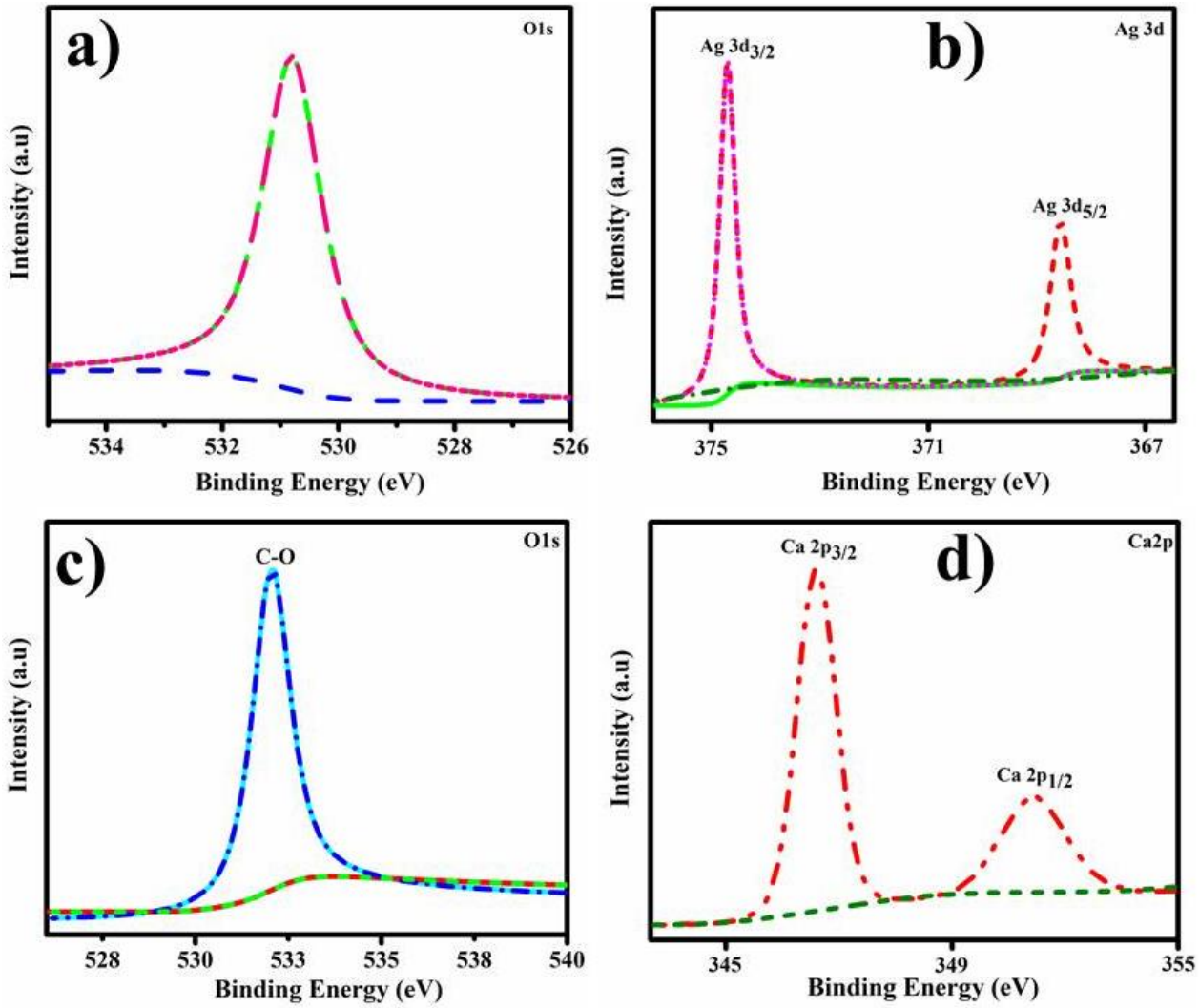

Figure S7 (a-d) XPS spectra of as prepared nanocomposites (a) Ag O1s (b) Ag 2p (c) CaO O1s (d) and Ca2p

The XPS spectra of Ag/CaO NCs doped with extract were investigated to determine the elemental structure and chemical state of the elements. Fig. S7 (a-d) shows the narrow scan XPS spectra of produced samples Ag O1s, Ag3d, Ca O1s, and Ca2p. The binding energy of Ag O1s was 530.8 eV for Ag/CaO NCs doped with extract Fig. S7(a), which is in good agreement with earlier findings [5, 6]. The location of the relevant binding energy peak was determined using the ionic and electronegativity properties of the atoms in the molecule. The binding energies of Ag^0 for the $Ag3d_{5/2}$ and $Ag3d_{3/2}$ orbits were 368.7 eV and 374.7 eV, respectively, see Fig. S7(b) [7]. The Ca O1s signal in the composite peak at 532.5 eV, which coincides with the C-O bond Fig. S7(c) [8]. Two peaks at 346.5 and 351.2 eV were discovered, corresponding to Ca $2p_{3/2}$ and Ca $2p_{1/2}$ in CaO, respectively, as shown in Fig. S7(d) [9].

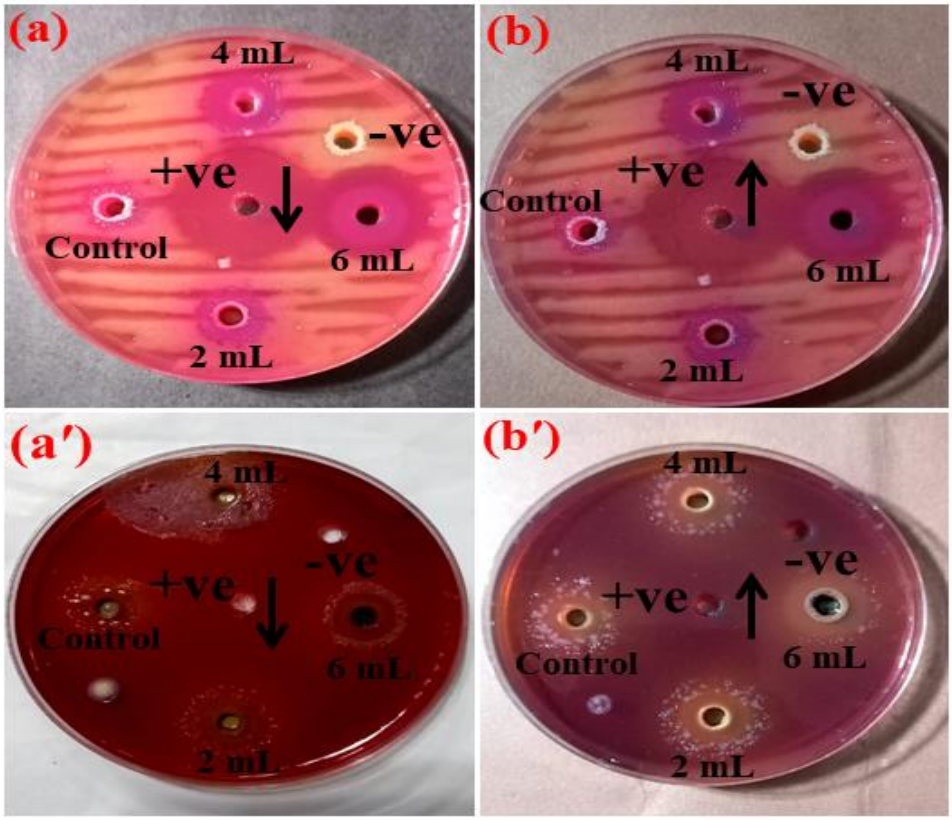

Figure S8. (a) *In-vitro* bactericidal efficacy of Ag/CaO, (b) 2 mL, (c) 4 mL , (d) 6 mL for *S. aureus*.

Table S1 Antimicrobial activity of Ag/CaO with different concentrations of extract

Samples	*S. aureus*		*E. coli*	
	Inhibition zone (mm)		Inhibition zone (mm)	
	0.5 mg/50 µL	1.0 mg/50 µL	0.5 mg/50 µL	1.0 mg/50 µL
Reference sample (Ag/CaO)	-	2.55	2.60	2.95
2 mL	-	4.65	3.40	3.05
4 mL	-	5.45	3.70	3.55
6 mL	0.90	9.15	4.70	6.30
Ciprofloxacin	10.15	10.15	7.25	7.25
DIW	0	0	0	0

Table S2 Surflex score of docked ligand Ag/CaO, SGL, and ZGN bonded to various molecular targets.

Protein	**Docking complex**	**CScore [a]**	**Crash score[b]**	**Polar score[c]**	**G score[d]**	**PMF score[e]**	**D score[f]**	**Chem score[g]**
S. aureus gyrase B	Ag/CaO	5.24	-0.08	4.52	-6.073	-2.283	-244.10	-8.332
	SGL	8.82	-2.28	3.45	-224.065	4.449	-72.010	-17.718
	ZGN	8.62	-1.03	5.78	-152.555	-16.688	-54.927	-12.631
S. aureus DHFR	Ag/CaO	5.85	-0.12	5.10	-3.947	0.335	-256.483	-5.480
	SGL	11.26	-2.51	6.62	-247.168	9.525	-85.315	-23.441
	ZGN	10.10	-0.85	7.74	-121.600	38.136	-27.547	-8.176
E. coli gyrase B	Ag/CaO	5.00	-0.01	3.99	-6.865	-0.711	-329.577	-5.480
	SGL	10.44	-2.50	2.21	-269.492	34.355	-74.975	-9.506
	ZGN	8.45	-2.49	5.15	-158.635	10.607	-29.947	-8.376
β-ketoacyl-[acyl carrier protein] synthase I (FabB)	Ag/CaO	5.52	-0.00	5.25	-1.167	-2.481	-212.050	-5.480
	SGL	8.81	-1.29	4.59	-198.429	19.129	-64.378	-7.742
	ZGN	6.18	-0.53	4.90	-92.839	35.318	-39.334	1.619
	TLM	5.56	-1.29	1.14	-149.828	66.698	-91.739	-11.155

[a]**CScore** is a consensus scoring which uses multiple types of scoring functions to rank the affinity of ligands, [b]**Crash**-score reveals the inappropriate penetration into the binding site, [c] **Polar** region of the ligand, [d] **G-score** shows hydrogen bonding, complex (ligand-protein), and internal (ligand-ligand) energies, [e] **PMF-score** indicates the Helmholtz free energies of interactions for protein-ligand atom pairs (Potential of Mean Force, PMF), [f] **D-score** for charge and van der Waals interactions between the protein and the ligand, [g] **Chem-score** points out hydrogen bonding, lipophilic contact, and rotational entropy, along with an intercept term.

REFERENCES

[1] Z. Mirghiasi, F. Bakhtiari, E. Darezereshki, E. Esmaeilzadeh, Preparation and characterization of CaO nanoparticles from Ca(OH)2 by direct thermal decomposition method, J. Ind. Eng. Chem. 20 (2014) 113–117. https://doi.org/10.1016/j.jiec.2013.04.018.

[2] M.Y. Abed, T.A. Hindia, M.G. Mohamed, A.M. Mazrouaa, Study on electrical conductivity of 2-vinylpyridine-methyl methacrylate copolymer in presence of cobalt acetate, J. Appl. Polym. Sci. 80 (2001) 2145–2153. https://doi.org/10.1002/app.1316.

[3] N. Prabhakarrao, M.R. Chandra, T.S. Rao, Synthesis of Zr doped TiO2/reduced Graphene Oxide (rGO) nanocomposite material for efficient photocatalytic degradation of Eosin Blue dye under visible light irradiation, J. Alloys Compd. 694 (2017) 596–606. https://doi.org/10.1016/j.jallcom.2016.09.329.

[4] X. Sun, K. Wang, Y. Shu, F. Zou, B. Zhang, G. Sun, H. Uyama, X. Wang, One-pot route towards active TiO2 doped hierarchically porous cellulose: Highly efficient photocatalysts for methylene blue degradation, Materials (Basel). 10 (2017). https://doi.org/10.3390/ma10040373.

[5] Y.H. Kim, D.K. Lee, H.G. Cha, C.W. Kim, Y.S. Kang, Synthesis and characterization of antibacterial Ag - SiO2 nanocomposite, J. Phys. Chem. C. 111 (2007) 3629–3635. https://doi.org/10.1021/jp068302w.

[6] Y. Sohn, SiO2 nanospheres modified by Ag nanoparticles: Surface charging and CO oxidation activity, J. Mol. Catal. A Chem. 379 (2013) 59–67. https://doi.org/10.1016/j.molcata.2013.07.015.

[7] H. Misran, M.A. Salim, S. Ramesh, Effect of Ag nanoparticles seeding on the properties of silica spheres, Ceram. Int. 44 (2018) 5901–5908. https://doi.org/10.1016/j.ceramint.2017.12.118.

[8] J. V. Rojas, M. Toro-Gonzalez, M.C. Molina-Higgins, C.E. Castano, Facile radiolytic synthesis of ruthenium nanoparticles on graphene oxide and carbon nanotubes, Mater. Sci. Eng. B Solid-State Mater. Adv. Technol. 205 (2016) 28–35. https://doi.org/10.1016/j.mseb.2015.12.005.

[9] J. Liu, M. Liu, S. Chen, B. Wang, J. Chen, D.P. Yang, S. Zhang, W. Du, Conversion of Au(III)-polluted waste eggshell into functional CaO/Au nanocatalyst for biodiesel production, Green Energy Environ. (2021). https://doi.org/10.1016/j.gee.2020.07.019.

Reviewer #1: The manuscript investigated the nanocomposite and their antimicrobial as well as catalytic reduction mechanism.

1. There are several typographical mistakes as well in whole manuscript. Therefore, the author's thoroughly careful check the language and typo mistake to minimize the error.

Ans: Corrected typos and other errors throughout the manuscript.

2. The abstract should be beginning with a sentence about the background of concept and the aims as well as novelty of study should be mentions. What exactly is the novelty of this study? The abstract is poorly written and should be improved. Abbreviations must be avoided in abstract. Parenthesis should be avoided in abstract - this is poor writing. Please improve.

Ans: The novelty of this research article has been added in the abstract as well as in the introduction section on page 4.

3. Introduction; Check and format the citations in the whole manuscript. Also, appropriate references must be provided to explained the background, what is already done and why this study carried out. Other vise the novelty of this research is still poorly presented. This is important especially for the high IF journals. The scientific style should be used. What exactly is the aim of this work? Hypothesis statement is missing in the introduction section.

Ans: Thanks for the constructive comment. Novelty, as well as a hypothesis, has been incorporated in the manuscript text on page no 4.

4. Results and discussion; General remark to the discussion - In my opinion, the discussion provided by Authors is difficult to follow and verify due missing critical details in the methodology section. Due to poorly described material and poorly presented methods, I am not able to follow and properly review the discussion. I would suggested to add following recent literature in the manuscript. https://doi.org/10.1016/j.chemosphere.2021.133056; https://doi.org/10.1016/j.colsurfb.2019.110734; https://doi.org/10.1016/j.ijbiomac.2021.05.202; and https://doi.org/10.1007/s10529-020-02795-3;

Ans: As per recommendation, we have added these references in the manuscript.

5. All figures are of poor technical quality and not suitable for publication, especially in a high reputed journal. Font size and kind is too small and must be unified in all figures. Small writings are unreadable. All figures must be self-explanatory. Axis titles are poorly presented or absent. Units are missing. Are the data presented in figures significantly different? At least error bars should be shown.

Ans: The quality of all figures has been improved by increasing the font size for easy and better understanding. We have also added bars in figure 5

6. I suggest first time write full name rather than abbreviation; revise throughout in manuscript

Ans: The full description of each abbreviation for the first time throughout the manuscript has been added.

Reviewer #2:
-The article's grammar and punctuation are not adequate and it needs to be deeply proofread.

Ans: Corrected accordingly per suggestions

-Going into details on the specific issues, here some comments are reported:
-All figure captions should be written in clear captions and mention results and discussion also. Some figures (supplementary documents) with results and discussions were not matched.

Ans: As per suggestions, all figure captions in the manuscript have been changed

-In Figure 2. The author should mention clear sample names.
-Figure 2 (a) XRD patterns……. (b) FTIR spectra……. and (c-d) SAED patterns of pristine CaO and extract doped Ag/CaO NCs and (e) representation of the unit cell of Ag/CaO.

Ans: For better and easy understanding, we have mentioned the name of each sample as per above recommendation.

In FTIR Figure2 should indicate significant peak values.

Ans: The significant peak values have been indicated in figure 2.

-The author noted 2.6 characterizations, The visual characteristics of materials were studied using a UV-vis spectrophotometer (Genesys 10S) in the wavelength spectrum of 180-400 nm. But the resulting graph In Fig. 3a. Ag exhibited a high peak window at 340-540 nm with maxima at 440 nm?

Ans: Thanks for the correction. In 2.6, the wavelength of UV-Vis spectrophotometer (Genesys 10S) has been corrected according to the resulting graph.

Figure 4 HR-TEM and interlayer d-spacing images of undoped CaO, Ag and extract doped Ag/CaO NCs.

Ans: Thanks for the correction. The caption of figure 4 has been changed for clear understanding.

(Fig. S1 (a- d)). But the figure shows the e and f also what about that figures?

Ans: Thanks for the correction. The caption of figure S1 has been changed for clear understanding.

Figure S1 EDS analysis of pure CaO, Ag and extract-doped Ag/CaO NCs. which is the pure

Ans: In figure, S1 (a) represents the pure CaO meanwhile, S1 (b) for pure Ag, S1 (c) for Ag-doped CaO, and (d-f) for 2 mL, 4 mL, and 6 mL extract doped Ag/CaO

-Antimicrobial effectiveness of Ag/CaO containing various concentrations of extract was obtained from zone of inhibition (ZOI) measurements through agar well diffusion assay against S. aureus (G +ve) and E. coli (G -ve) pathogens as shown in Fig. S4 but figure shows Figure S4 Schematic diagram of antimicrobial mechanism. What about the ZOI?

Ans: Corrected in the manuscript text.

Highlights

- A low temperature Green synthesis of Ag/CaO nanocomposites (NCs) was prepared.
- Various concentrations of extract (*Zingiber officinale*) into NCs.
- The optimum amount of extract in NCs showed effective MB:CF dye degradation.
- The doped NCs showed strong antimicrobial activity against *E. coli,* and *S. aueus*.
- A new pathway to produce extract doped Ag/CaO materials as low cost catalyst.

Graphical Abstract

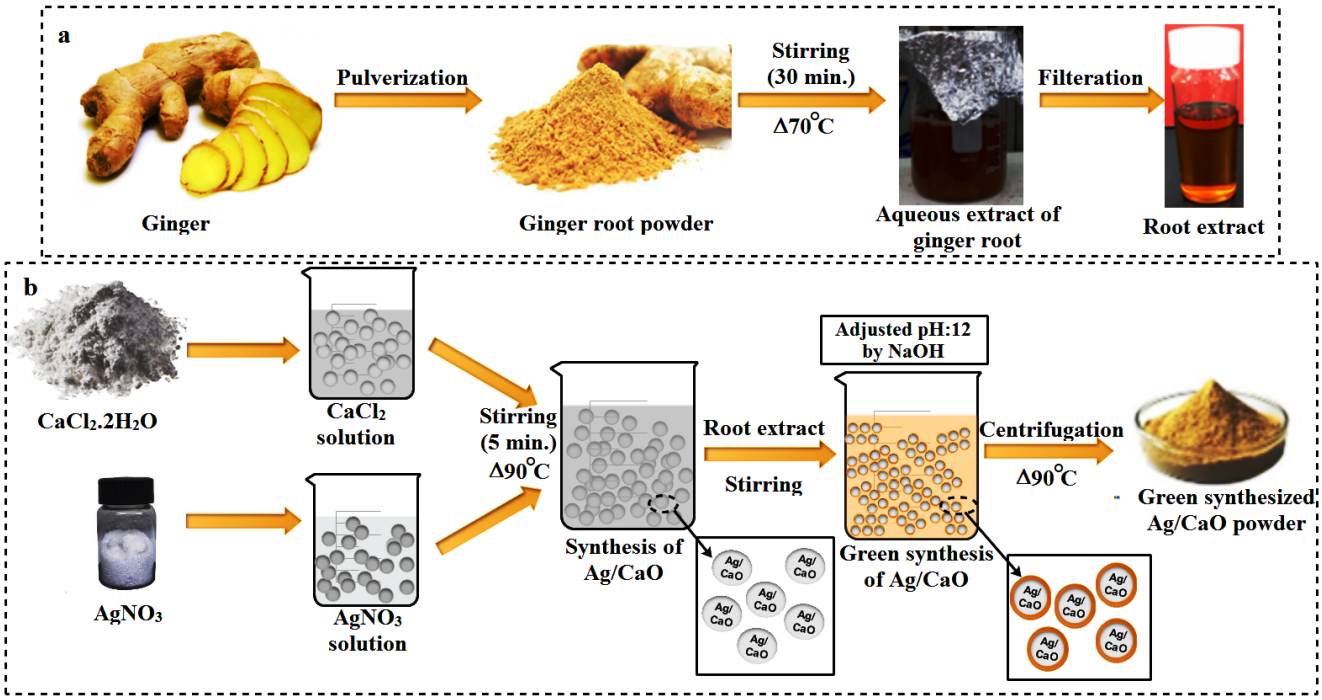

Figure 1 Schematic diagram of (a) Extraction of ginger root (b) synthesis of green synthesized Ag/CaO NCs.

Declaration of interests/Conflict of Interest

☒ The authors declare that they have no known competing financial interests or personal relationships that could have appeared to influence the work reported in this paper.
This manuscript has no conflict of interest

Dr. Muhammad Ikram
Assistant Professor Physics
GC University Lahore